CHALMERS
UNIVERSITY OF TECHNOLOGY

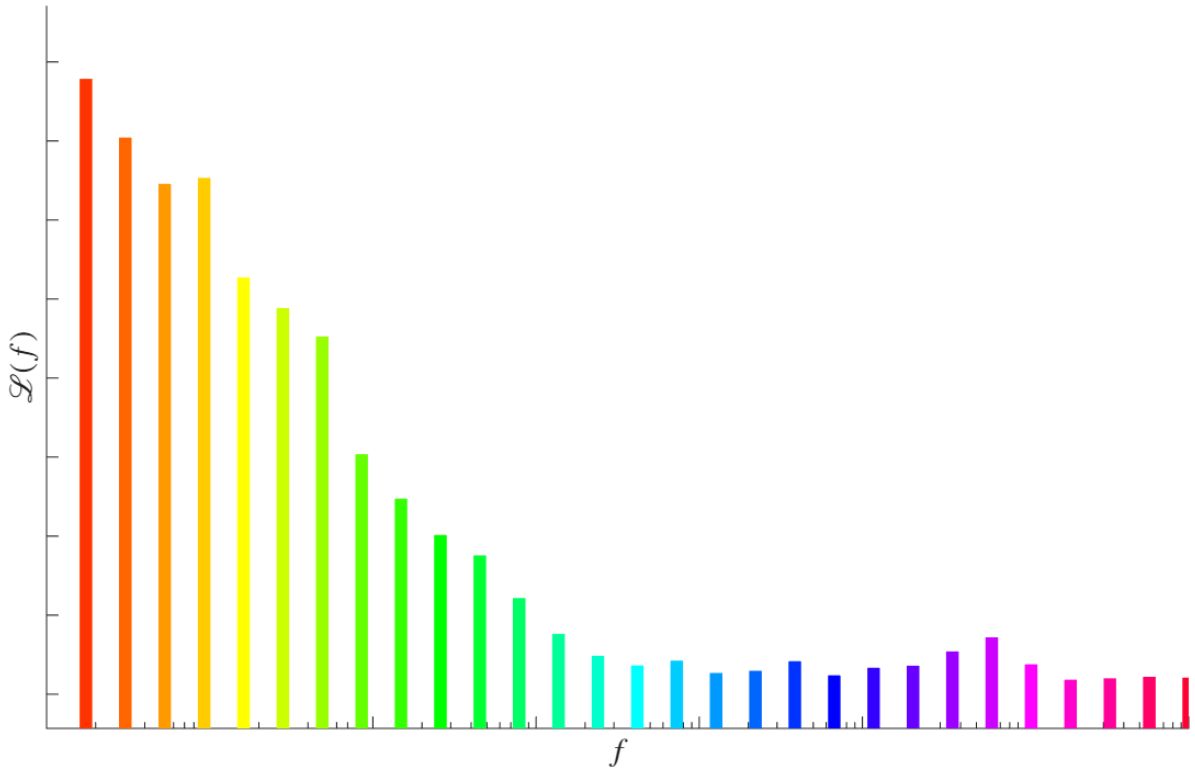

Optical Oscillator Evaluation in Radio Test Bed

Integration and Phase Noise Characterization of a Microresonator-Based Optical Oscillator

Master's thesis in Wireless, Photonics and Space Engineering

DAVID HISELIUS

DEPARTMENT OF ELECTRICAL ENGINEERING

CHALMERS UNIVERSITY OF TECHNOLOGY
Gothenburg, Sweden 2026
www.chalmers.se

Master's thesis 2026

Optical Oscillator Evaluation in Radio Test Bed

Integration and Phase Noise Characterization of a Microresonator-Based Optical Oscillator

DAVID HISELIUS

CHALMERS
UNIVERSITY OF TECHNOLOGY

Department of Electrical Engineering
Division of Microtechnology and Nanoscience (MC2)
Chalmers University of Technology
Gothenburg, Sweden 2026

Optical Oscillator Evaluation in Radio Test Bed
Integration and Phase Noise Characterization of a Microresonator-Based Optical Oscillator
DAVID HISELIUS

Academic Supervisor: Dan Kuylenstierna, Microtechnology and Nanoscience
Industrial Supervisors: Mikael Hörberg, Johan Karlsson, Ericsson AB
Examiner: Dan Kuylenstierna, Microtechnology and Nanoscience

Master's Thesis 2026
Department of Electrical Engineering
Division of Microtechnology and Nanoscience
Chalmers University of Technology
SE-412 96 Gothenburg
Telephone +46 31 772 1000

Cover: Stylistic representation of phase noise using optical frequency comb lines.

Typeset in LaTeX
Printed by Chalmers Reproservice
Gothenburg, Sweden 2026

Optical Oscillator Evaluation in Radio Test Bed
Integration and Phase Noise Characterization of a Microresonator-Based Optical Oscillator
DAVID HISELIUS
Department of Electrical Engineering
Chalmers University of Technology

Abstract

Local oscillator (LO) phase noise presents significant challenges in achieving high-capacity wireless communication at millimeter-Wave frequencies. Through optical frequency division (OFD), high-Q resonators may be leveraged to generate low phase noise microwave frequency signals. In this work, Kerr microresonator-based OFD was integrated as an LO source in a point-to-point link radio test bed. The frequency divider and amplifier used to facilitate integration of the optical oscillator into the radio test bed were characterized from a phase noise perspective. The optical oscillator was subsequently analyzed by correlating observations in the phase noise spectrum to known noise mechanisms. Finally, radio link performance for external local oscillator sources, including the optical oscillator under study, was compared to an unmodified channel. Results indicate that photodetection noise constituted the primary performance limitation of the optical oscillator implementation, resulting in a comparatively high phase noise floor (-145 dBc/Hz). The impact of noise introduced by the frequency divider and amplifier on radio link performance is estimated to be minor; however, residual phase noise measurements are required to verify this assumption. In radio link measurements, the optical oscillator achieved signal-to-noise ratios approximately 6 dB lower than those of the unmodified channel. The observed degradation in radio link performance is consistent with previous studies identifying the LO noise floor as a dominant limitation in wideband communication systems. As the oscillator demonstrated excellent near-carrier phase noise (-130 dBc/Hz @ 100 kHz) and established methods of photodetection noise mitigation exist, further investigation is warranted.

Keywords: optical frequency division, microwave photonics, phase noise, local oscillator

Acknowledgements

I would like to give a heartfelt thank you to the people involved in this work.
My academic supervisor and examiner Dan Kuylenstierna enabled a supportive environment of encouragement and open discussion.
The work was carried out in collaboration with Ericsson AB, who provided access to not only equipment necessary for project realization, but perhaps more importantly supervision by Mikael Hörberg and Johan Karlsson. Mikael gave an insight into industrial research, and always took the time to discuss and explain theoretical concepts. Through practical device and lab experience, Johan was likely responsible for the successful implementation of the optical oscillator in the radio test bed. Without the many constructive discussions with both Mikael and Johan, work would have been exponentially harder.
A special thanks also goes out to Ashish K. Adiga. His work in construction of the optical oscillator as well as supporting the electrical system implementation made this work possible.
Finally, I want to thank my friends and family who have supported me through my educational journey. Without you, I wouldn't be able to present my work here today.

David Hiselius, Gothenburg, June 2026

List of Acronyms

Below is the list of acronyms that have been used throughout this thesis listed in alphabetical order:

AM	Amplitude Modulation
CML	Current-mode Logic
CP	Charge Pump
CW	Continuous Wave
DUT	Device Under Test
DKS	Dissipative Kerr Soliton
EVM	Error Vector Magnitude
FD	Frequency Divider
FWM	Four-wave Mixing
IF	Intermediate Frequency
LNA	Low-noise Amplifier
LO	Local Oscillator
NA	Not Available
OFD	Optical Frequency Division
PD	Phase Detector
PLL	Phase Locked Loop
PM	Phase Modulation
PNA	Phase Noise Analyzer
PSD	Power Spectral Density
RF	Radio Frequency
RIN	Relative Intensity Noise
RMS	Root Mean Square
RU	Radio Unit
Rx	Receiver
SCL	Source-coupled Logic
SINR	Signal-to-Interference-plus-Noise Ratio
SNR	Signal-to-Noise Ratio
Tx	Transmitter
VCO	Voltage-controlled Oscillator
VOP	Velocity of Propagation

Contents

List of Figures

List of Tables

1

Introduction

Wireless communication has become an indispensable part of modern society, and demand for wireless capacity continues to increase. By increasing carrier frequencies into millimeter-wave (mmWave) regions, high absolute bandwidths can be achieved. In high frequency, high bandwidth communication, local oscillator (LO) phase noise now presents a significant bottleneck [5].

High orders of modulation with densely spaced constellation points become especially sensitive to phase noise degradation, making oscillator noise a critical performance parameter. Improvements in LO spectral purity may therefore result in substantial performance benefits.

At high carrier frequencies, conventional electronic oscillator architectures face fundamental challenges related to device noise, resonator quality factors, and power consumption. As a result, photonics-based approaches for microwave and mmWave signal generation have gained increasing attention. Optical oscillators inherently exhibit low phase noise due to their high quality-factor resonators and reduced sensitivity to electronic noise mechanisms. By transferring the spectral purity of an optical source to the radio-frequency (RF) domain, photonics-based oscillators provide a promising pathway for generating low-phase-noise RF signals.

1.1 Electronic Frequency Synthesis

Current-day frequency synthesis is typically achieved using phase-locked loops.

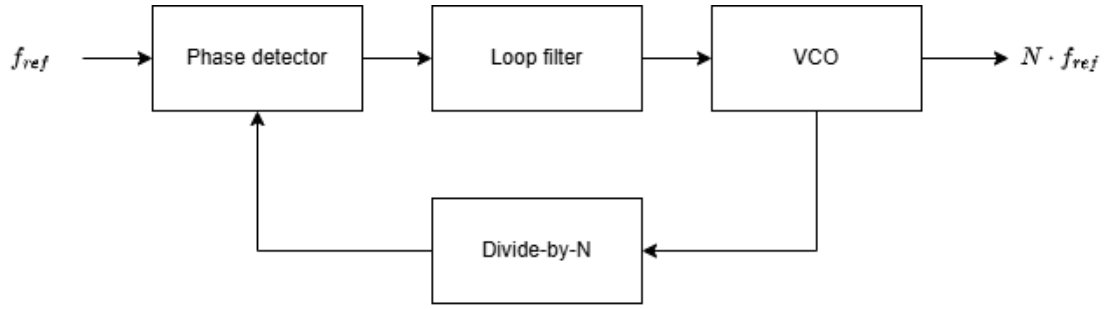

Figure 1.1: Basic phase-locked loop voltage-controlled oscillator configuration.

A phase-locked loop (PLL) is a feedback phase and frequency synchronizing system. By comparing the PLL output signal with a known reference, the frequency can be adjusted. When synchronized, the system is said to be *locked*.

Fig. 1.1 shows a typical phase-locked loop (PLL) configuration. A phase detector (PD) is used to compare the reference signal with the PLL output. To compare the phase between reference and output signal, frequency division of the feedback output signal is used. Based on the phase difference detected by the PD, the voltage-controlled oscillator (VCO) can be steered: adjusting the output frequency such that it is locked to the reference. In modern PLL's, charge pumps are often used.

The reference signal is typically generated using a frequency stable high quality crystal oscillator. Within the PLL bandwidth, phase noise performance is largely determined by the reference source, while the out-of-band phase noise is dominated by the intrinsic noise of the VCO resonator [37].

Sources of noise in PLL circuits include VCO-, frequency divider- and phase detector noise. Further analysis of PLL noise can be found in [13].

The output frequency of a PLL is limited by the voltage-controlled oscillator (VCO). To achieve high carrier frequencies, frequency multiplication is often required. When frequency multiplication is performed, phase fluctuations are essentially magnified.

1.2 Optical Frequency Division

Microwave photonics is a discipline that combines the fields of radio-frequency engineering and photonics. Recent advancements in integrated microwave photonics (IMWP), driven by progress in materials science, nanofabrication, and photonic integration, have enabled the development of compact, lightweight, and cost-effective components [3].

Optical frequency division (OFD) is a technique used in microwave photonics in order to generate high stability microwave frequency signals. OFD is achieved using optical frequency combs, consisting of a set of mutually coherent optical tones with

precisely defined frequency spacing. Beat frequencies between adjacent comb lines can be detected using high speed photodiodes to generate an RF signal at the comb repetition rate, the frequency of which only limited by the photodetector bandwidth [40]. This enables direct generation of microwave and mmWave signals with potentially low phase noise and high spectral purity [20].

An inherent benefit of OFD relates to the quality-factor advantage of optical resonators. Oscillator phase noise is highly dependent on the resonator quality factor Q [22]. Optical resonators typically achieve quality factors Q in the order of 10^6 to 10^8, several orders of magnitude greater than their electrical counterparts. Microwave and mmWave signals generated through OFD have been demonstrated to exhibit phase noise performance comparable to, or exceeding, that of the best available microwave oscillators [11].

1.3 Project aim

The aim of this project is to study the integration of a Kerr microresonator-based optical oscillator into a radio communication test bed and evaluate the resulting radio link performance through phase noise analysis.

To address this aim, the thesis seeks to answer the following research questions:

- How can an optical oscillator be integrated as a local oscillator source in a radio test bed?
- What is the phase noise impact of the components needed for integration?
- Can we estimate radio link performance based on local oscillator phase noise?
- What limits the phase noise performance of the optical oscillator as a local oscillator in a wideband communication link?

2

Phase Noise

This chapter begins by introducing fundamental concepts of phase noise and jitter. A theoretical derivation of noise shaping in oscillators is then presented, followed by a characterization of oscillator phase noise regions. Subsequently, a method for introducing white phase noise is described.

Implementation of the optical oscillator in the radio test bed necessitated frequency division. Frequency division and electrical frequency dividers are therefore studied from a phase noise perspective.

Phase noise is the random fluctuations in the phase of a periodic signal. An ideal oscillator produces a periodic signal at an oscillation frequency f_0, which can be expressed as

$$V(t) = V_0 \cdot cos[2\pi f_0 t], \tag{2.1}$$

where V_0 and f_0 are the nominal amplitude and frequency respectively.

In the frequency domain, this corresponds to a spectral line at $\pm f_0$. In a practical oscillator, amplitude noise (AM noise) and phase noise (PM noise) will result in some amount of energy being distributed in the sidebands around the carrier frequency.

The output of a noisy oscillator can be expressed as

$$V(t) = [V_0 + \varepsilon(t)] \cdot cos[2\pi f_0 t + \phi(t)], \tag{2.2}$$

where $\varepsilon(t)$ is the fractional amplitude fluctuation and $\phi(t)$ the phase fluctuation in units of [rad]. $\phi(t)$ is commonly treated as a zero-mean stationary random process [22]. $S_\phi(f)$ is the single-sided power spectral density (PSD) of phase variations in units of rad^2/Hz.

Phase noise is quantified as the single-sideband-phase-noise-to-carrier ratio $\mathcal{L}(f)$:

$$\mathcal{L}(f) = \frac{S_\phi(f)}{2} \tag{2.3}$$

where f denotes the Fourier frequency offset from the carrier frequency. $\mathcal{L}(f)$ is often given in units of decibel relative to carrier, $\mathcal{L}(f) = 10\log_{10}(S_\phi(f)/2)$ [dBc/Hz].

2.1 Jitter

In the time domain, phase noise manifests itself as jitter.

Jitter is defined as “a general term that describes a phenomenon consisting in the deviation of the reference instants of a sequence of events from their ideal values" [17].

Jitter affecting timing reference signals, such as clock signals, is referred to as timing jitter. When characterized in terms of statistical distribution or time trends, timing jitter is expressed in units of time or unit interval (UI).

The amplitude of the timing jitter is defined as the range of deviations of the actual reference instants of a timing waveform from their ideal values.

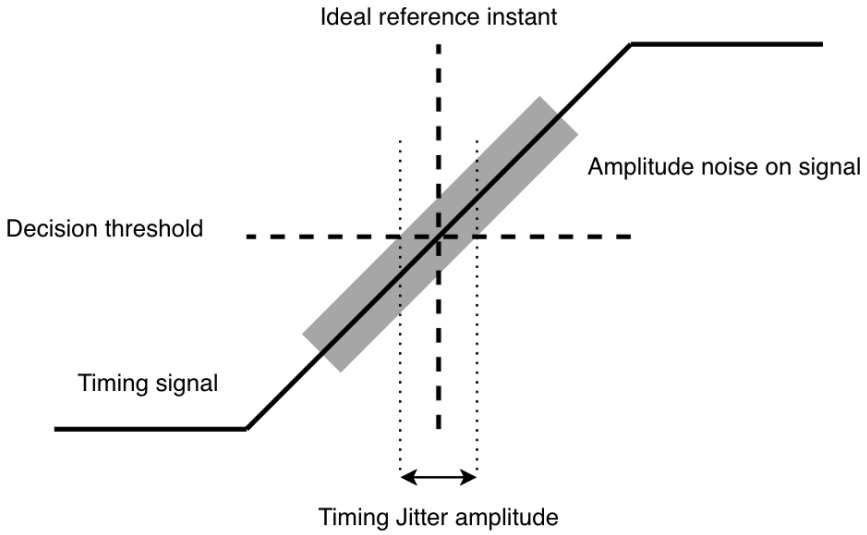

Figure 2.1: Timing jitter induced by additive amplitude noise.

Fig. 2.1 illustrates timing jitter induced by additive amplitude noise.

Jitter may be subdivided into random and deterministic jitter. Random jitter is uncorrelated and analogous to white phase noise when observed in $S_\phi(f)$ (Fig. 2.5). It can thus only be described statistically, and is modeled as a zero-mean process with Gaussian distribution.

Deterministic jitter is unlike random jitter not intrinsic, and its causes can theoretically be determined. Deterministic jitter can be further subdivided into periodic jitter (PJ) and data-dependent jitter (DDJ). DDJ describes signal data pattern deviations due to effects such as inter symbol interference and duty cycle distortion. This work is primarily concerned with reference signals, and DDJ is therefore not studied further.

Depending on the source of noise, PJ may be correlated or uncorrelated [17]. Causes include transmission line cross-talk and electromagnetic interference. A switching power supply will introduce periodic noise at the switching frequency of operation [33]. Periodic spurious noise, often referred to simply as "spurs", can be seen in

phase noise measurement through narrow-band peaks.

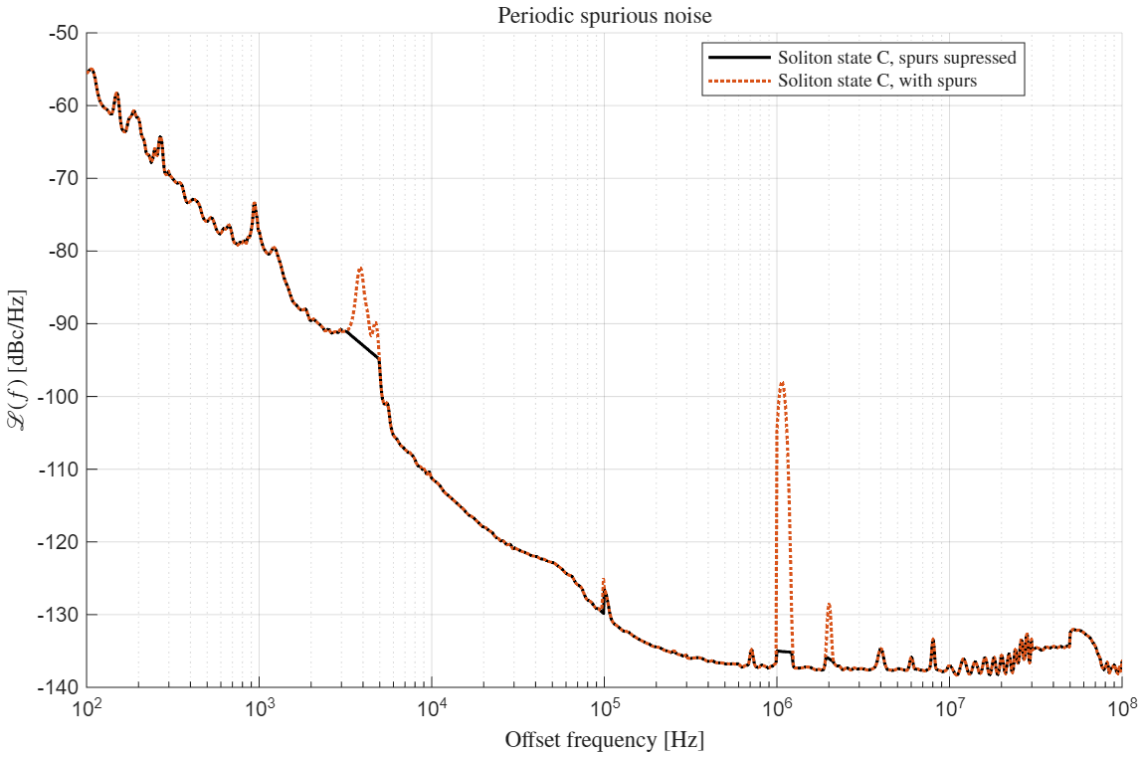

Figure 2.2: Periodic spurious noise, Soliton State C.

Figure 2.2 shows the phase noise of *Soliton State C* (see section 5.2) with and without suppression of spurious noise. When measured, large spurs are often suppressed to improve result visualization.

The resolution bandwidth (RBW) describes the bandwidth of the intermediate frequency (IF) filter in a spectrum- or phase noise analyzer (PNA). Within the RBW, the spectrum energy is normalized. In a PNA, the RBW is typically dynamically adjusted. The RBW is reduced for lower offset frequencies, and increased for higher offset frequencies to reduce measurement time. Narrow-band spurs occurring at high frequency offsets may therefore be incorrectly normalized.

The root mean square (RMS) phase over a noise bandwidth $f_b - f_a$ can be calculated through integration of $S_\phi(f)$:

$$\phi_{\text{rms}} = \sqrt{\int_{f_a}^{f_b} S_\phi(f)\, df} = \sqrt{2\int_{f_a}^{f_b} \mathcal{L}(f)\, df}. \tag{2.4}$$

The RMS phase jitter $J_{\phi,\text{rms}}$ in time units is given by equation (2.5):

$$J_{\phi,\text{rms}} = \frac{\phi_{\text{rms}}}{2\pi f_0} \tag{2.5}$$

The RMS phase ϕ_{rms} and system SNR can be approximately correlated through

$$\text{SNR} = -20\log_{10}(\phi_{rms}). \tag{2.6}$$

We define SNR_ϕ as the phase-noise-limited-signal-to-noise-ratio in this work. SNR_ϕ is derived using equation (2.6) for a given ϕ_{rms}.

2.2 Oscillator Noise Shaping

An oscillator is a fundamentally nonlinear system. When a circuit begins to oscillate, it's signal amplitude grows until limited by open-loop gain. However, if the signal swing is sufficiently small, a linear system approximation may be valid [29]. In [29], the following derivation for phase noise shaping is found.

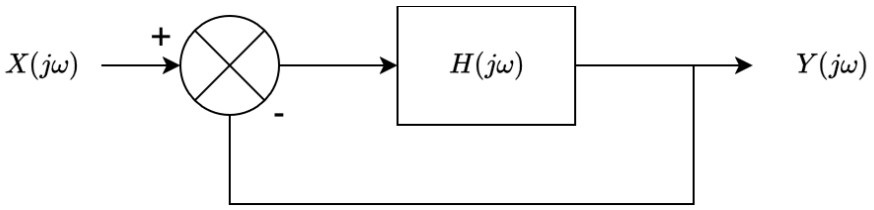

Figure 2.3: Linear oscillator system model

To analyze phase noise, we model an oscillator as a feedback system, shown in Fig. 2.3.

The system transfer function is

$$\frac{Y}{X}(j\omega) = \frac{H(j\omega)}{1 + H(j\omega)} \tag{2.7}$$

Oscillation is achieved when the transfer function tends to infinity. This occurs for $H(j\omega_0) = -1$, known as the *Barkhausen criterion*. The total phase shift of the feedback loop is therefore 2π, resulting in constructive interference.

At frequencies close to the carrier frequency, $\omega = \omega_0 + \Delta\omega$, equation (2.7) can be approximated as

$$H(j\omega) \approx H(j\omega_0) + \Delta\omega \frac{dH}{d\omega}. \tag{2.8}$$

The noise transfer function is therefore estimated as

$$\frac{Y}{X}[j(\omega_0 + \Delta\omega)] = \frac{H(j\omega_0) + \Delta\omega \frac{dH}{d\omega}}{1 + H(j\omega_0) + \Delta\omega \frac{dH}{d\omega}} \tag{2.9}$$

When oscillation is achieved, $H(j\omega_0) = -1$. With $\Delta\omega \frac{dH}{d\omega}$ generally being small, the noise transfer function can be approximated as

$$\frac{Y}{X}[j(\omega_0 + \Delta\omega)] \approx \frac{-1}{\Delta\omega \frac{dH}{d\omega}} \tag{2.10}$$

The resulting phase noise PSD therefore takes the shape of

$$\left|\frac{Y}{X}[j(\omega_0+\Delta\omega)]\right|^2 = \frac{1}{(\Delta\omega)^2\left|\frac{dH}{d\omega}\right|^2}. \tag{2.11}$$

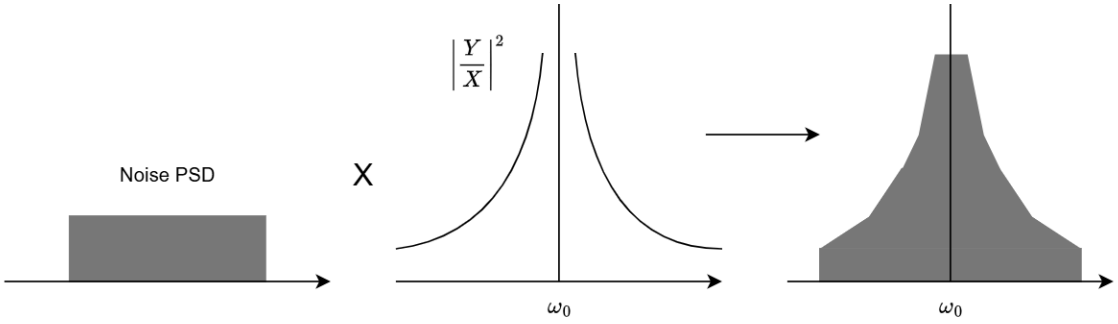

Figure 2.4: Noise shaping in oscillators, [29] (Fig. 8).

The process of noise forming is seen in Fig. 2.4, where the noise PSD is formed in accordance with equation (2.11).

2.3 Oscillator Noise Regions

Noise mechanisms of oscillators can be observed in the PN spectrum by categorizing distinct noise regions.

The Polynomial Law or Power Law can be used to characterize regions of phase noise described by negative exponent polynomials.

$$S_\phi(f) = \sum_{i\leq -4}^{0} b_i f^i \tag{2.12}$$

Regions described by the polynomial law are seen in Fig. 2.5.

To study the regions of S_ϕ, suppose a random noise $i(t)$ current with power spectral density containing both flicker phase and white phase regions is injected into an oscillator node. Noise components near integer multiples of ω_0 transform to low frequency phase noise sidebands [14]. Flicker noise in $i(t)$ give rise to $1/f^3$ or white frequency noise. White noise in $i(t)$ give rise to $1/f^2$ and $1/f$ noise terms in $S_\phi(f)$.[1]

Oscillator noise includes all regions of slope. Other two-port devices can only exhibit flicker phase and white phase noise.

Long-term oscillator frequency change is commonly known as frequency *drift*. Drift can occur due to changes in oscillator components, environment variables, load and power supply changes [16].

[1]Derivation in: *A General Theory of Phase Noise in Electrical Oscillators*, A. Hajimiri [14].

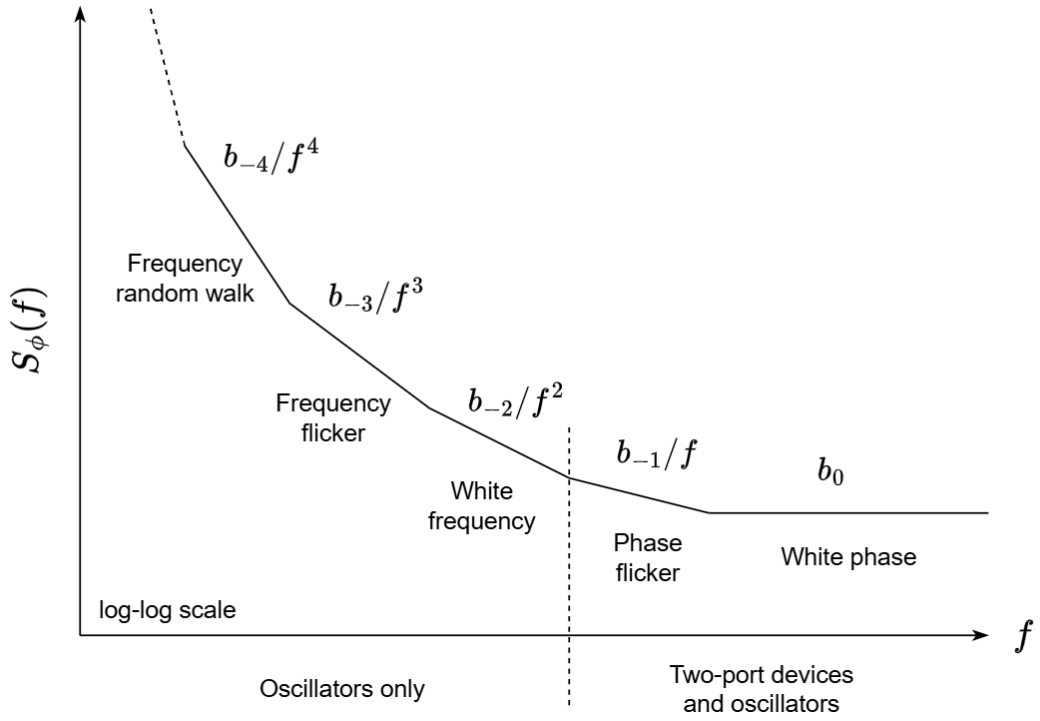

Figure 2.5: Polynomial law phase noise spectrum.

2.3.1 Noise Floor Elevation

The white phase noise floor has been verified experimentally to be one of the main limiting factors in high frequency, high bandwidth system performance [5]. Due to the significant impact, system performance insight may be gained by elevating the white phase noise floor.

The noise figure F describes the degradation in signal-to-noise between the input and output of a system. Expressed using the equivalent temperature T_e and system temperature T_0, the noise figure is

$$F = 1 + \frac{T_e}{T_0}. \tag{2.13}$$

If a components output noise exhibits low or no frequency dependence, it can be modeled as an equivalent noise temperature T_e [26]. A lossy component such as an attenuator has an equivalent noise temperature

$$T_e = \frac{1-G}{G}T = (L-1)T \tag{2.14}$$

where G is the component gain, $L = 1/G$ the equivalent loss and T the device temperature. It follows that a X-dB attenuator will have a noise figure of $F = X$ dB for $T = T_0$. As such, attenuation and subsequent amplification with a net signal gain of 0 dB may therefore be employed to elevate the phase noise floor.

Suppose a signal exhibits phase noise at thermal noise level. The thermal noise

PSD $S_n = k_B T \approx -174$ dBm/Hz for $T = 290$ K. Since the noise power cannot be attenuated below the thermal noise floor, attenuating and subsequently amplifying such a signal will result in worsening of phase noise performance as the noise power is amplified. Hence, the SNR will be reduced by the factor of attenuation.

A signal with a phase noise floor higher than the thermal noise floor may exhibit a different response: attenuating such a signal will attenuate both the signal and noise.

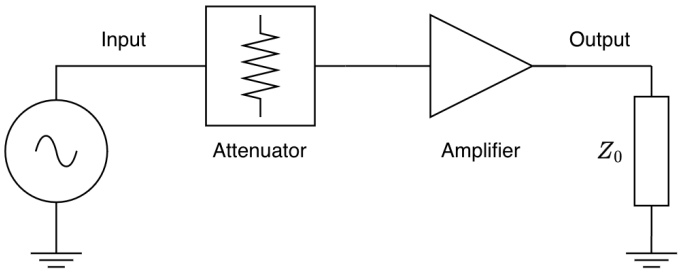

Figure 2.6: Schematic representation of the simulation setup used to evaluate noise floor elevation.

To illustrate the effect of the proposed noise floor elevation, a simulation is performed in *Keysight* Advanced Design System (ADS). A functional representation is seen in Fig. 2.6. An oscillator source with phase noise impairment was introduced using the *OSCwPhNoise* component. The oscillator output signal is attenuated by a lossy attenuator with $T = T_0 = 290$ K. Ideal amplification is introduced resulting in a net 0 dB gain, and the signal phase noise is measured at the output node terminated with a matched load.

Fig. 2.7 shows simulation results of noise floor elevation performed using the simulation environment described in Fig. 2.6. The amount of phase noise introduced is seen to depend on the level relative to the thermal noise floor. Phase noise at levels higher than the elevated noise floor is unaffected.

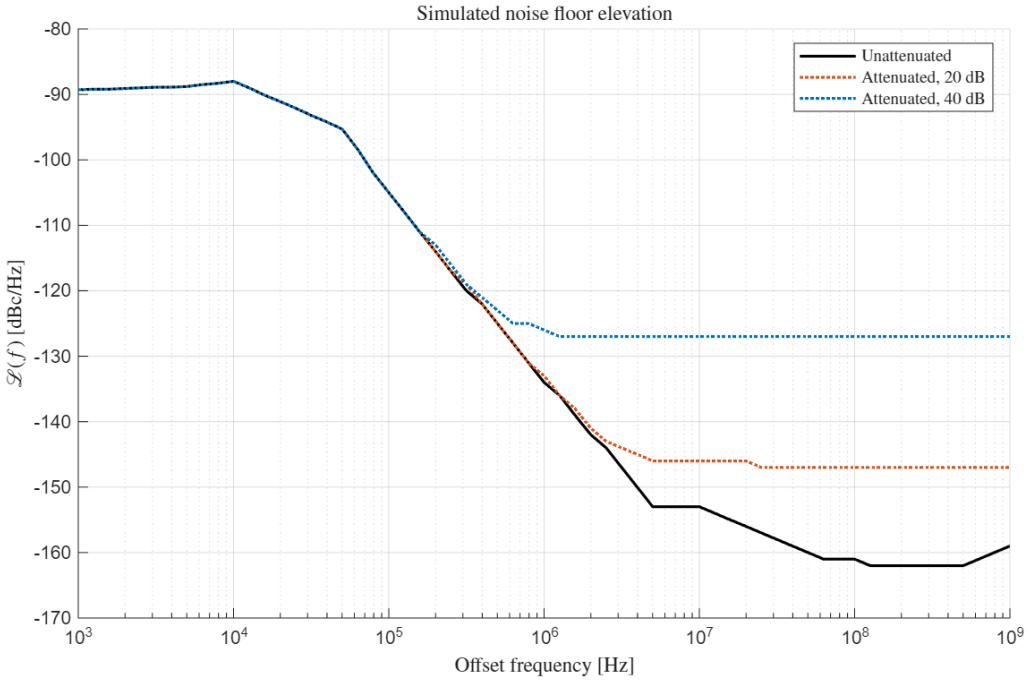

Figure 2.7: Simulated noise floor elevation as a function of attenuation/amplification.

2.4 Frequency division

Ideal frequency division inherently results in a decrease in phase noise. Omitting amplitude fluctuations, frequency division by a factor N applied to equation (2.2) can be expressed as

$$V(t) = V_0 \cdot cos[(2\pi f_0/N) \cdot t + \phi(t)/N]. \tag{2.15}$$

As $\mathcal{L}(f)$ scales quadratically with phase fluctuations, frequency division results in a phase noise improvement by $1/N^2$ or $-20\log(N)$ dB. This phenomenon can be observed through the output/input phase PSD $S_o(f) = S_i(f)/N^2$, as described in [9].

2.4.1 Source-coupled Logic Frequency Dividers

Source-coupled logic (SCL), also known as current-mode logic (CML), is a digital design technique using steering of a constant-current source between paired transistors. A differential logic input is applied to normally depletion mode field-effect transistors (FETs). This method of frequency division is referred to as *digital* or *static*. Static frequency dividers operating at high frequencies commonly employ CML [38].

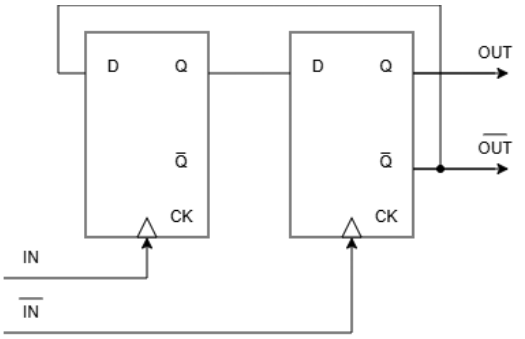

Figure 2.8: Asynchronous D-latch divide-by-2 topology.

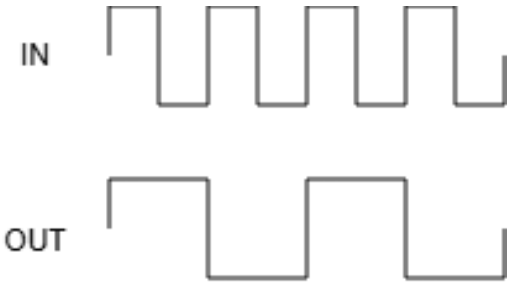

Figure 2.9: Time diagram of asynchronous D-latch divide-by-2.

An asynchronous SCL leader-follower divide-by-2 D-latch topology can be seen in Fig. 2.8. A differential input signal is applied to the clock (CK) inputs of the D-latches. The output signal of the follower stage is fed back into the leader stage data (D) input. Divide-by-N can be achieved through cascading of divide-by-2 circuits. Both synchronous and asynchronous division can be realized.

Fig. 2.9 shows the time diagram of the input/output signal for a divide-by-2 divider. On the rising edge of the input signal, the leader D-latch is enabled and loads the input data, while on the falling edge the follower D-latch is enabled and updates the output.

Static dividers introduce white phase and flicker phase noise. For asynchronous static frequency dividers, jitter at the divider output is the quadratic sum of the jitter of each latch [23]. Intrinsic transistor parameters and device implementation impacts the significance of noise contributions on the additive phase noise of the divider. FET's typically generate a significant amount of flicker noise. Flicker noise introduced by amplification stages may fold into the PN PSD, provided that the corner frequency of the noise bandwidth is higher than the input signal frequency [23].

Power supply noise may also influence the threshold voltage and rise/fall time in digital dividers [7]. Switched mode power supplies operating at high switching frequencies introduce electromagnetic interference (EMI). Interference present in timing and frequency-processing circuits such as oscillators and frequency dividers can be upconverted to the phase noise sidebands.

2.4.2 Injection-locked Frequency Dividers

A common method of frequency division in mmWave systems is the injection-locked frequency divider (ILFD).

ILFDs operate by synchronizing an oscillator with an injected signal v_i. According to [28], three classes of injection-locked oscillators (ILO's) can be defined: first-harmonic, subharmonic and super-harmonic. In first-harmonic ILO's, the oscillator frequency is locked to the external signal [1]. For subharmonic and superharmonic ILO's, the incident signal is a subharmonic and harmonic of the oscillator frequency

respectively. Superharmonic ILO's can therefore be used to realize frequency division.

A fundamental limitation of ILFDs is the narrow operational bandwidth due to the requirement on frequency locking. The maximum deviation between the incidence- and oscillator frequency for which locking occurs depends on the input/output signal amplitude and resonance factor [1]. Techniques to increase ILFD bandwidth have been studied, but frequency locking range remains narrow when compared to static dividers [18].

2.5 Residual phase noise

Residual phase noise, also known as additive phase noise, is the added phase noise contribution when a signal passes through a device. In [10], Egan investigates "processing of noise modulation by the phase-locked loop" and defined the phase noise transfer function (PNTF) as

$$H(f) = \frac{\phi_{tot} - \phi_{res}}{\phi_{in}} \tag{2.16}$$

where ϕ_{tot} is the total PN at the device output, ϕ_{res} is the residual PN at the device output, ϕ_{in} is the PN at the device input.

If special consideration to measurement setup is not taken, the phase noise measured is the absolute phase noise ϕ_{tot}. The residual phase noise of a DUT cannot be extracted from absolute phase noise, containing multiple sources of noise.

For many devices, such as passive components, amplifiers, and frequency multipliers, full transfer of the input phase noise to the output can be assumed. In contrast, ideal frequency division modifies the phase-noise transfer characteristic and provides an inherent phase-noise reduction.

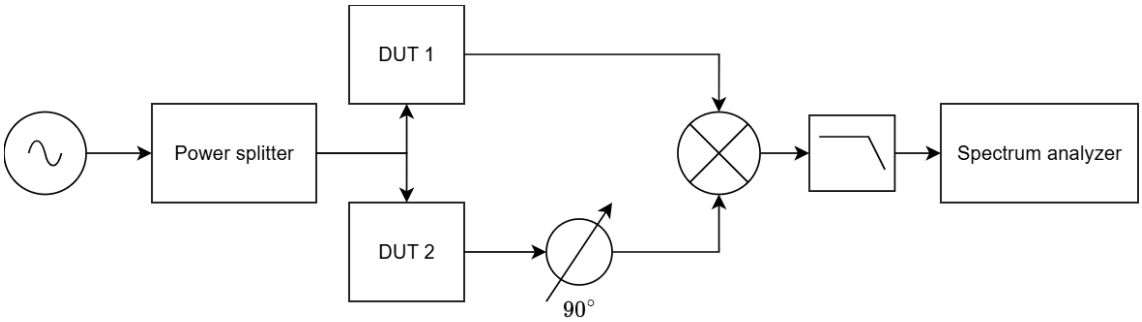

Figure 2.10: Residual phase noise measurement setup.

Residual phase noise measurements are typically performed using two DUT's. A commonly employed residual phase noise measurement setup is seen in Fig. 2.10. The output signal of the DUT's are fed to a balanced mixer in quadrature, achieving phase detection. The phase detected signal is thereby demodulated, and the output phase noise is the sum of the residual phase noise of both DUT's.

3

Optical Oscillator

Although not the primary focus, the optical oscillator forms the backbone of the system studied in this work. In this chapter, theoretical concepts of optical frequency division (OFD) are introduced. The mechanism behind the generation of an optical frequency comb used in this work is briefly described. Photodetection allows the transition between the optical and electrical domain. However, it also introduces key performance limitations. Consequently, the phase-noise contributions arising from photodetection are analyzed in detail, with particular emphasis on noise mechanisms in high-speed photodetectors relevant to OFD systems.

For in-depth information on concepts outlined here, further reading is encouraged: [15, 20, 41, 27].

3.1 Optical Frequency Division

Optical frequency division (OFD) is the process in which the fractional frequency stability of an optical oscillator is transferred to a lower-frequency signal through coherent division. An optical frequency comb (OFC) is a uniformly spaced grid of discrete spectral lines, seen in Fig. 3.1. In the time domain, the OFC corresponds to a pulse train whose repetition frequency is equal to the spectral line spacing. Since the optical carrier frequency is many orders of magnitude higher than the repetition frequency, the comb effectively acts as a coherent frequency divider.

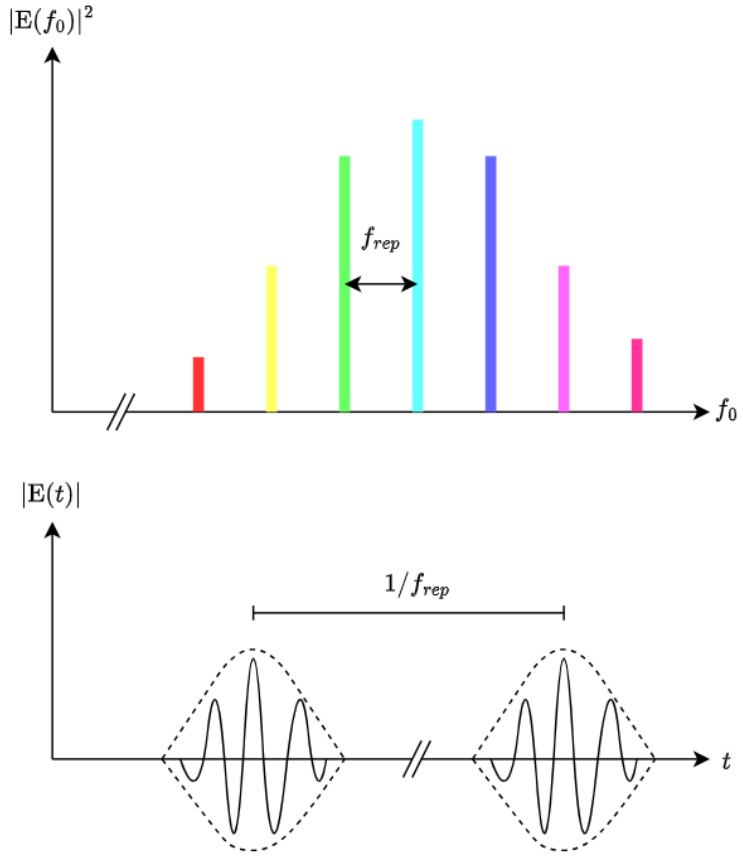

Figure 3.1: Optical frequency comb and corresponding time-domain pulse train.

In this work, a high-Q Si_3N_4 microresonator is used to generate a *Kerr* optical frequency comb. The Kerr nonlinearity is a change in material refractive index dependent on the optical power. Si_3N_4 is a nonlinear, dispersive optical medium which enables Kerr nonlinear interactions. The dominant mechanism underlying Kerr comb generation is four-wave mixing (FWM) in which two photons of frequencies ω_1 and ω_2 annihilate, generating two new photons at ω_3 and ω_4. As the process of FWM repeats, the OFC is formed [41].

The microresonator used in this work is a *coupled photonic cavity*, often called a *photonic molecule*. The photonic molecule used is described in [15].

When a continuous-wave laser is input to the microresonator, a dissipative Kerr soliton (DKS) can be formed through the balance of dispersion and nonlinearity, as well as the (parametric) gain and cavity loss [41]. Multi-soliton states in which two or more solitons co-propagate can also be attained. A higher number of Kerr solitons was experimentally observed to generate a higher output signal power, later shown to have significant impact on system performance (see sections 5.2 and 5.3).

3.1.1 2-point Optical Frequency Division

In 2-point OFD, an auxiliary laser is injected. A comb "tooth" sufficiently close to the auxiliary laser frequency will then be "pinned", and the OFC will inherit the relative frequency stability of the auxiliary laser [19]. The spectral separation between pump and auxiliary laser translate to a division ratio, and the repetition rate pulse train will in turn experience a phase noise reduction by the square of the division ratio,

$$\mathcal{L}_{\text{rep}}(f) = \mathcal{L}_{\text{opt}}(f) - 20\log_{10}\left(\frac{\Delta\nu}{f_{\text{rep}}}\right) \tag{3.1}$$

where $\Delta\nu$ is the spectral separation frequency of the comb teeth, $\mathcal{L}_{\text{rep}}(f)$ is the phase noise of the repetition rate signal and $\mathcal{L}_{\text{opt}}(f)$ the optical phase noise of the pump laser.

3.2 Photodetection

In OFD systems, the operation of the high-speed photodiode is critical for achieving low-noise microwave signals. Excess shot- and flicker- noise, as well as nonlinear signal distortion in photodetection can quickly nullify any advantages of photonic techniques.

A fast photodiode with a bandwidth covering f_{rep} is used to detect the pulse train to generate a photocurrent at the microcomb pulse repetition rate. Square-law detection converts incident optical intensity into photocurrent as

$$I(t) \propto |E(t)|^2, \tag{3.2}$$

where $E(t)$ is the optical field envelope incident on the detector and $i(t)$ is the detector photocurrent.

The photocurrent is accompanied by several noise contributions. Assuming a photodetector amplifier with source impedance R_s the thermal (Johnson–Nyquist) noise current PSD is given by

$$S_T = \frac{4k_BT}{R_s}. \tag{3.3}$$

3.2.1 Shot-noise

Photodetection typically generates high levels of shot noise. As the photocurrent scales quadratically with the incident field amplitude, optical power plays a significant role in reducing the influence of shot-noise.

Shot-noise occurs due to the discrete nature of charge carriers in electrical currents. The shot noise level and subsequent SNR of high speed photodetectors is often limited by power handling capabilities [27].

Assuming stationary conditions, the shot-noise current PSD is given by

$$S_i = 2qI, \tag{3.4}$$

where q is the fundamental charge and I is the average photocurrent.

The output photocurrent is found as $I = RP_L$, where R is the photodetector responsivity and P_L the optical (laser) input power. The shot noise PSD is therefore

$$S_n = 2qRP_L. \tag{3.5}$$

The photodetector used in this work was the Coherent's XPDV2120r ([6]). Assuming a matched load $R_L = 50\ \Omega$ and $P_L = 10$ dBm, the RF noise PSD is ≈ -160 dBm/Hz. This optical power corresponds to the maximum average optical input power for which the XPDV2120r photodetector exhibits a linear response. For these operating conditions, the repetition rate RF signal output power was observed to be approximately -10 dBm, resulting in a shot-noise limited phase noise of -150 dBc/Hz.

The electrical power scales quadratically with photocurrent through

$$P_{\mathrm{RF}} = \frac{I_{\mathrm{RF}}^2 R_L}{2} \tag{3.6}$$

It is therefore clear that improvements in shot-noise can be achieved using higher optical input powers.

3.2.2 AM-to-PM Noise

For ultrashort pulse detection as seen in OFD applications, pump laser relative intensity noise (RIN) results in AM-to-PM noise conversion [8]. AM-to-PM noise, also known as amplitude to phase conversion (APC) is a major performance bottleneck in ultra-low noise optoelectronics [4].

An empirical model describes the RIN induced phase noise through

$$\mathcal{L}_{\mathrm{RIN}}(f) = 10 \cdot \log_{10}[S_I(f)] + 20 \cdot \log_{10}[\alpha] - 3 \tag{3.7}$$

where $S_I(f)$ is the one-sided power spectral density of the low frequency relative intensity fluctuations of the laser and α a coefficient indicating the rejection of APC. Under saturation, α ranges from 0.3 - 3 in InGaAs PIN photodiodes [4].

4

Methods

This chapter aims to describe the methods used to characterize the optical oscillator implementation. First, the measurements of frequency divider phase noise and amplifier gain are detailed. The construction of a simplified radio test bed is thereafter described. Four measurement configurations are presented, allowing radio link performance to be related to LO signal parameters. Finally, the implementation of the optical oscillator in the radio test bed is shown.

4.1 Frequency Divider Characterization

This section explains the steps taken to characterize the frequency divider employed in the radio test bed. The input power sensitivity, here defined as the minimum input power at which frequency division is performed, and the output power were measured and compared with the manufacturer's specifications. Phase noise measurements were also performed, enabling a comprehensive assessment of the divider's performance.

Frequency division was performed using the AT-FDN-54AS2-FD divide-by-N (N=2-256) programmable frequency divider from *AT Microwave*. The divider can be used with a differential or single-ended input signal. The output signal of the optical oscillator generated by photodetection is single-ended. Therefore, all subsequent testing is done using a single-ended input/output signal.

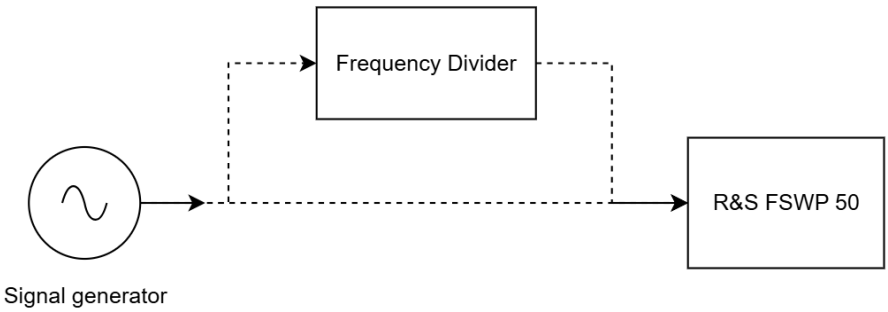

Figure 4.1: Frequency divider phase noise measurement setup.

An initial test of functionality was performed using the measurement configuration seen in Fig. 4.1. A continuous wave (CW) input signal generated by the Anritsu

MG3695B signal generator. The unused input/output ports of the frequency divider were terminated. Reference measurements were performed by omitting the frequency divider, indicated by dashed lines.

Functionality was confirmed for varying division factors $N = 2$, 4, 8 and 16 within the datasheet specified input frequency range.

4.1.1 Input power sensitivity and output power

To facilitate integration of the frequency divider into the radio test bed, its input power sensitivity and output power were characterized and compared with datasheet specifications. First, the relationship between the signal generator output power and the power delivered to the divider input was established through calibration measurements. Using this calibration, the minimum input power required for correct frequency division was determined by gradually reducing the input power until the divider ceased to operate.

The measured input power sensitivity and output power were found to be in agreement with the datasheet specifications [24].

4.1.2 Phase noise

The phase noise of the signal generator was measured using the R&S FSWP phase noise analyzer (PNA). Phase noise was measured for all signal generator output power levels previously used in power characterization.

Phase noise measurements are absolute, i.e. no residual phase noise measurements are performed. Limitations in available devices (one) prevented usage of the commonly employed residual phase noise measurement setup shown in Fig. 2.10.

4.2 Amplification

An initial hypothesis was that the output power of the photodetector in the optical oscillator would be insufficient for proper operation of the FD in the radio test bed. Therefore, electrical amplification was required. In order to reduce the unwanted effects of electrical amplification on the oscillator performance, minimal noise contribution should be introduced.

The noise figure, defined as the reduction in input/output SNR dictates the level of additive white noise. For an amplifier with noise figure F, the white phase noise of a signal is

$$S_\phi(f) = \frac{Fk_bT}{P_0} \tag{4.1}$$

where T is the temperature and P_0 is carrier power [31]. It follows that an amplifier with low noise figure is desirable when minimizing white phase noise contributions.

Amplifiers also introduce $1/f$ (flicker phase) noise. The level of $1/f$- noise is rarely specified by manufacturers, and is therefore often confirmed experimentally [31].

Another important parameter is the 1-dB compression point. The 1-dB compression point marks the point at which the amplifier exhibits nonlinear properties. When reached, the signal will start to experience distortion [12]. Finally, sufficient gain was needed.

The ADL8106 low-noise amplifier (LNA) was chosen due to it's high gain and relatively low noise figure at 50 GHz, as well as coaxial interfacing on the EVAL-ADL8106 evaluation board.

The process of noise floor elevation described in section 2.3.1 requires attenuation and gain such that a net zero gain is achieved. Due to bandwidth limitations of the LNA, the SHF 806 E modulator driver was used. Amplifier usage in the radio test bed are described in sections 4.3 and 3.

Datasheet specifications for amplifiers used in this work are seen in Table 4.1. No noise figure is specified for the SHF 806 E.

Table 4.1: Amplifier specifications.

Amplifier	Typ. Gain [dB]	Noise Figure [dB]	Frequency range
ADL8106	20.5	4	18 - 54 GHz
SHF 806 E	26	NA	40 kHz - 38 GHz

In order to verify LNA performance, gain was measured under input power conditions representative of those encountered in radio testbed applications.

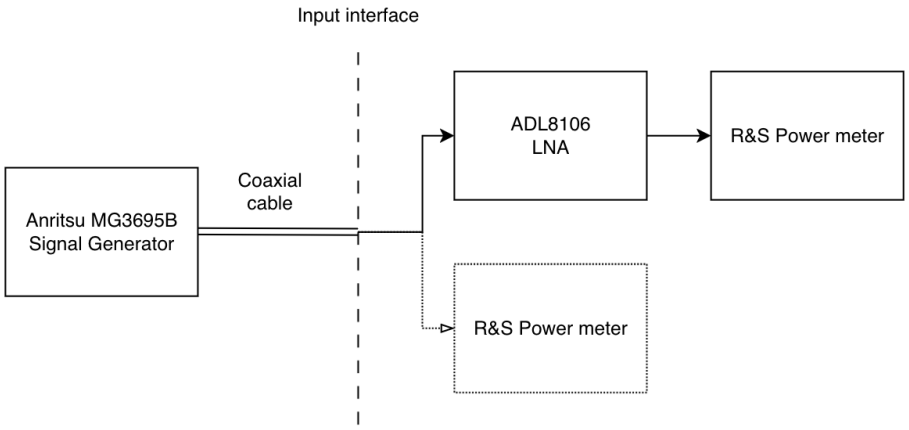

Figure 4.2: LNA gain and 1-dB compression measurement setup.

Fig. 4.2 shows the measurement setup used to perform gain and 1-dB compression measurements.

The measurement setup is shown in Fig. 4.2. A CW RF signal at 50 GHz was generated using the Anritsu signal generator. The displayed output power was incremented in steps of 2 dB from -20 dBm to +6 dBm. The RF power was recorded for all measurement points. The LNA was thereafter introduced and power measurements were performed at the output.

Resulting LNA gain and input/output power is seen in Fig. 4.3. The measured gain follows the nominal gain as stated in the ADL8106 datasheet [2] to a large extent. The total deviation of gain over the measurement interval is 0.2 dB. For the frequency range 50 - 54 GHz, the datasheet specified nominal Output 1dB Compression Point (OP_{1dB}) is 19 dBm. In this measurement series, a maximum output power of 14.6 dBm was observed with no significant gain reduction visible.

As the estimated and observed signal power in subsequent system configurations is low relative to the values measured here, we can therefore likely assume that signal distortion due to LNA compression is unlikely to occur.

The noise figure was not experimentally confirmed.

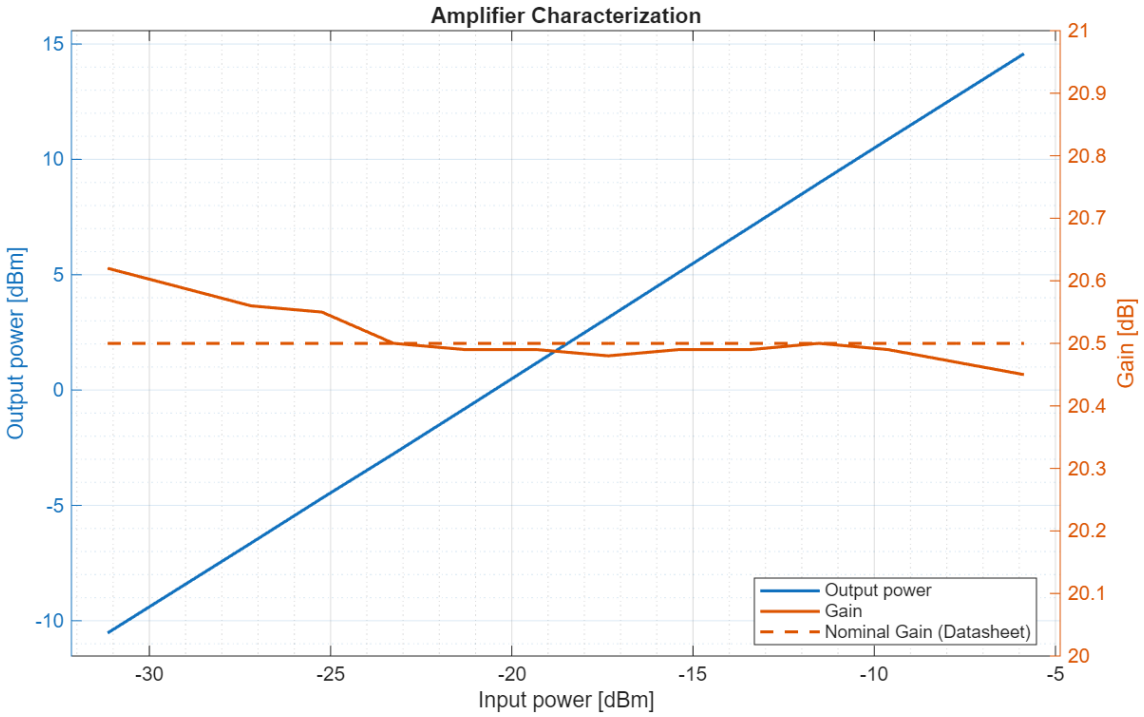

Figure 4.3: LNA gain, input/output power and datasheet specified nominal gain, $f_0 = 50$ GHz.

4.3 Radio Test Bed

The radio test bed forms the supporting architecture to evaluate the optical oscillator in a radio communication link. Two point-to-point radio units (RUs) operate as a full-duplex link in the E-band frequency range. In a point-to-point link, the notion of up/down-link is arbitrary. Here, we denote the link at RF frequency 75 GHz as the uplink. The downlink is separated by 10 GHz, and operates at 85 GHz.

The radio units used in this project employ homodyne, also known as zero-intermediate frequency, conversion for link bandwidths of 1000, 1500 and 2000 MHz. At lower link bandwidths, an intermediate frequency (IF) stage is introduced in superheterodyne conversion. The IF differs between Tx/Rx RU in the radio link, enabling effective filtering of LO leakage. In the radio test bed, a single LO signal is injected in both RU's. This limited the available bandwidths to 1000, 1500 and 2000 MHz.

In order to evaluate the performance of the optical oscillator as an LO source, the internal LO signal in the uplink must first be intercepted, and the hardware modified such that an external signal can be injected.

Information on components used in the RU's is not public. The RU internal LO signal will therefore be referred to as Internal PLL.

Fig. 4.4 shows extrapolated closed-loop phase noise data from datasheet specification for the internal PLL LO used in the RU's. Internal implementation parameters such as reference oscillator and loop bandwidth may influence the phase noise.

The PLL output is filtered before being applied to the mixer stage. The external LO

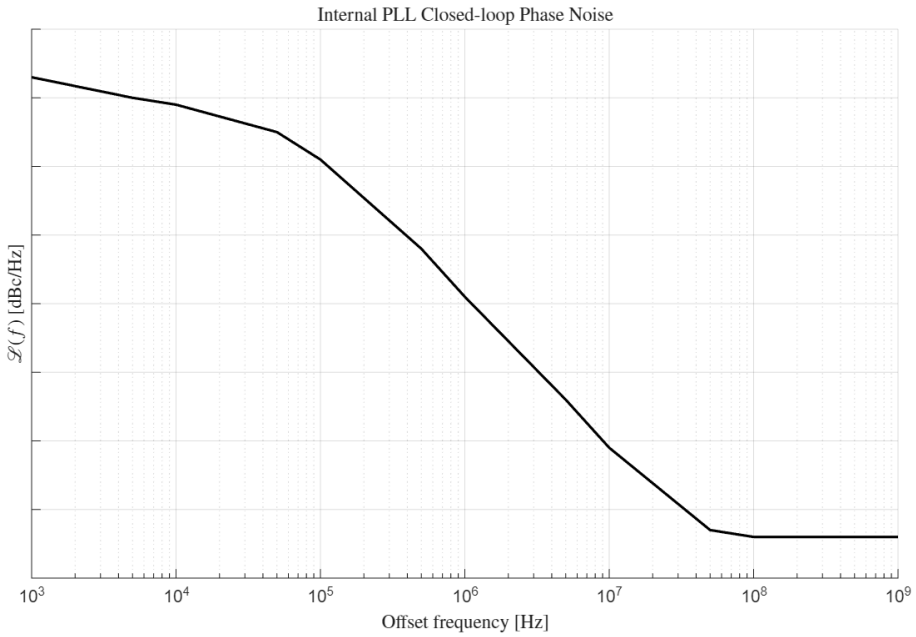

Figure 4.4: Internal PLL Closed-loop phase noise.

signal was injected after the filter which was electrically disconnected. The internal PLL output was disconnected from the filter input and terminated using a 50 Ω resistor.

An initial radio test bed was thereafter constructed, a functional diagram can be seen in Fig. 4.5.

In order to investigate the correlation between LO phase noise and radio communication performance, several system configurations were used to modify the characteristics of the LO signal.

The configurations used were:

1. **Correlated**
   No attenuator or amplifier is included between the signal generator and power splitter. The output branches of the split signal are of equal length.
2. **Correlated, ADL8106**
   The ADL8106 LNA is connected between the signal generator output and power splitter input. The output branches of the split signal are of equal length.
3. **Correlated, SHF 806 E**
   A 20 dB attenuator is placed before the SHF 806 E amplifier. This configuration aims to achieve noise floor elevation (see sections 2.3.1 and 5.3.1). The output branches of the split signal are of equal length.
4. **Uncorrelated**
   No attenuation or amplification is performed. The split signal is thereafter fed to the LO input port using different length cables. De-correlation is discussed in section 4.3.1.

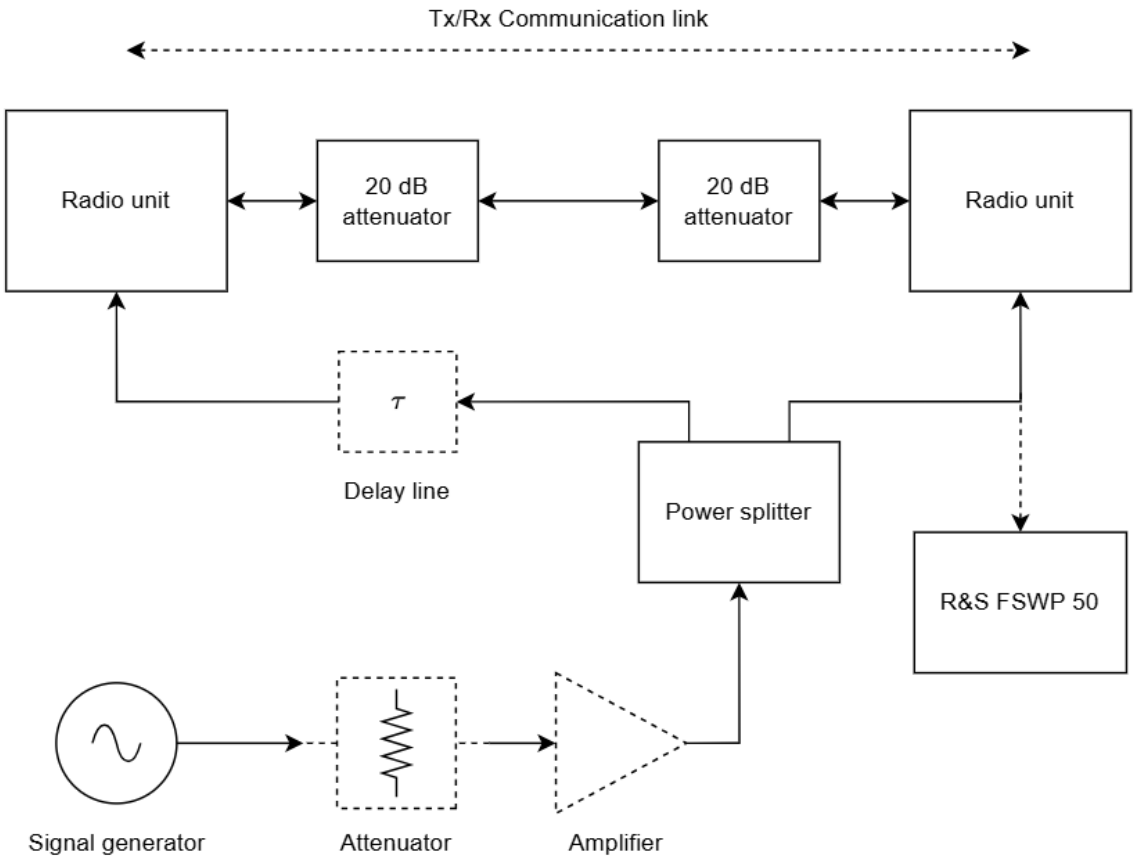

Figure 4.5: Radio test bed, signal generator LO source. A dotted frame/trace is used to indicate components/connections not always present.

Two signal generators were used: the Anritsu MG3695B and the Rohde & Schwarz SMB100A. They are hereafter denoted simply as "Anritsu" and "Rohde & Schwarz", respectively. For all measurement series, a CW signal at $f_0 = 12.5$ GHz was used, approximately matching the output frequency of the optical oscillator implementation (see section 3). All radio test bed measurements made using a signal generator were performed at three output power levels. Power levels were chosen such that phase noise performance variation could be clearly observed, whilst maintaining a functional radio link.

Phase noise measurements were performed at the RU LO interface to correlate phase noise- and radio link performance. During phase noise measurements, the signal is disconnected from the radio unit and instead fed to the PNA as indicated in Fig. 4.5 right hand side.

Figure 4.6 shows the phase noise of the signal generators used in the radio test bed at three output power settings. Variations in signal generator output power is commonly achieved using variable attenuation. A lower output power, as a result of higher signal attenuation, can be seen to have a large influence on the noise floor.

For each radio link bandwidth, varying signal generator output powers were used. The output power of the signal generator directly relates to the phase noise floor

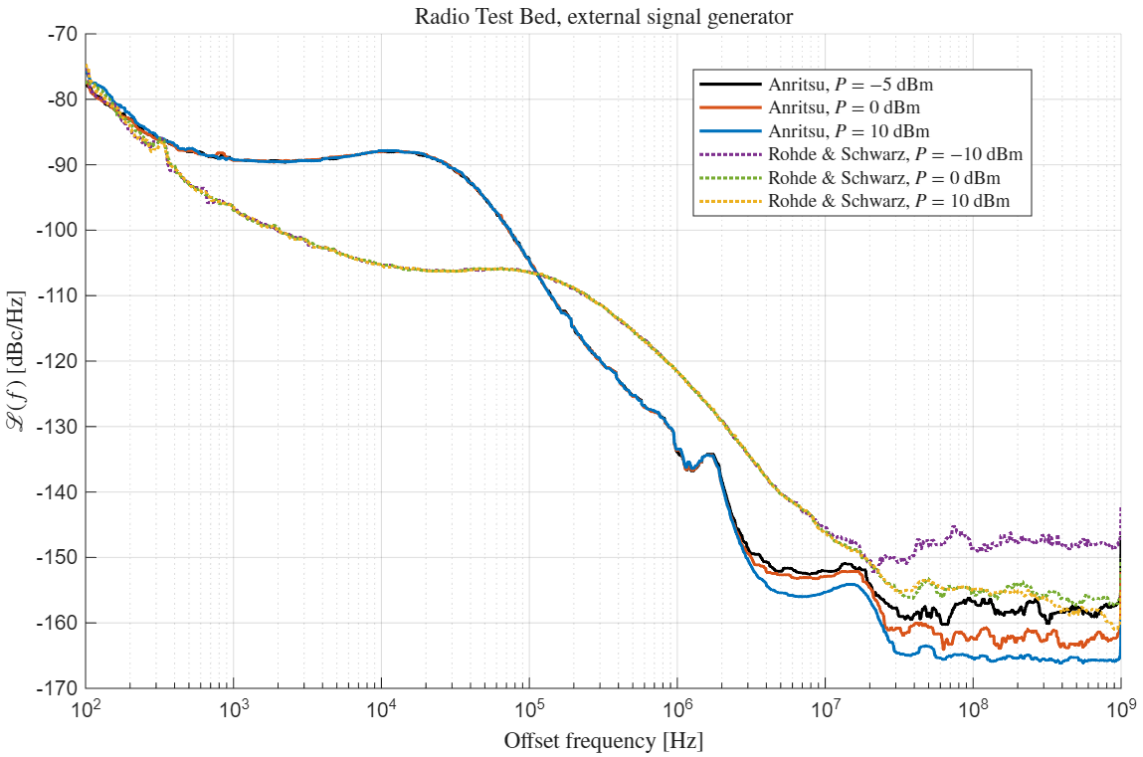

Figure 4.6: Phase noise of signal generators used in radio test bed measurements. Indicated signal power refers to the output power level indicated on the signal generator.

of the signal, as the thermal noise relative to the signal level increases with lowered carrier power. This can be seen in Fig. 4.6.

In order to perform noise floor degradation as described in section 2.3.1, the signal must be first attenuated and thereafter amplified by an equal amount. At $f_0 = 12.5$ GHz, the LNA operated outside its specified range. Under these conditions, the amplifier gain was significantly reduced, and the inclusion of the LNA resulted in an overall negative net gain (loss). Therefore, the SHF 806 E amplifier was introduced.

4.3.1 Signal de-correlation

In a wireless link, the Tx/Rx LO noise spectrum are uncorrelated.

When implemented in the radio test bed, a single optically generated RF signal was split using a power divider and fed to both RU's in phase. Therefore, an investigation on the effects of noise correlation on radio link performance is warranted.

In order to simulate an environment with uncorrelated phase noise, de-correlation was performed by altering the branch length of the split LO signal through the introduction of the delay line τ in Fig. 4.5.

Observing the LO signal in the time domain, any instance of timing error will be delayed by the transmission time of the signal through the signal path. Given sufficient difference in electrical length of the signal branches, de-correlation can be assumed. In [32], it is shown that frequency offsets $f \leq 1/6\tau$ are de-correlated.

With a physical length difference in transmission line of 50 cm and velocity of propagation (VOP) of 80%, the time difference is found as

$$\tau = \frac{L}{c_0 \cdot VOP} = \frac{0.5}{c_0 \cdot 0.8} \approx 2 \cdot 10^{-9}. \tag{4.2}$$

Frequency offsets below $f \leq 1/(6{\cdot}2{\cdot}10^{-9}) \approx 83$ MHz are therefore de-correlated. For signal sources used in de-correlation measurements, seen in Fig. 4.6, any correlated noise has therefore been de-correlated.

4.4 Optical oscillator

The Toptica CTL 1550 laser was used to drive the microcomb resonator. Phase noise measurements of the laser source repetition rate signal used in the optical oscillator, recorded using the OEwaves OE4000 laser characterization system, was provided.

To reference the observed performance of the implemented oscillator, a theoretical estimation of achievable 2-point OFD phase noise performance was calculated, referred to as the *theoretical OFD limit*. Using equation (3.1) with a spectral separation $\Delta\nu \approx 2.49$ THz and $f_{rep} = 49.92$ GHz resulted in a phase noise reduction of ≈ 34 dB. An approximate shot-noise limit of -150 dBc/Hz, derived in section 3.2.1, was used to estimate the white phase noise floor of the ideal OFD.

It should be noted that **2-point locking was not performed** during subsequent measurements as it was found to worsen phase noise performance.

When implemented in the radio test bed, optical oscillator phase noise was measured at the RU LO port interface (Fig. 4.8) at a carrier frequency $f_0 = 12.48$ GHz. The theoretical OFD limit was therefore scaled to 12.5 GHz by applying equation (2.15) with a division factor of 4 (-12 dB).

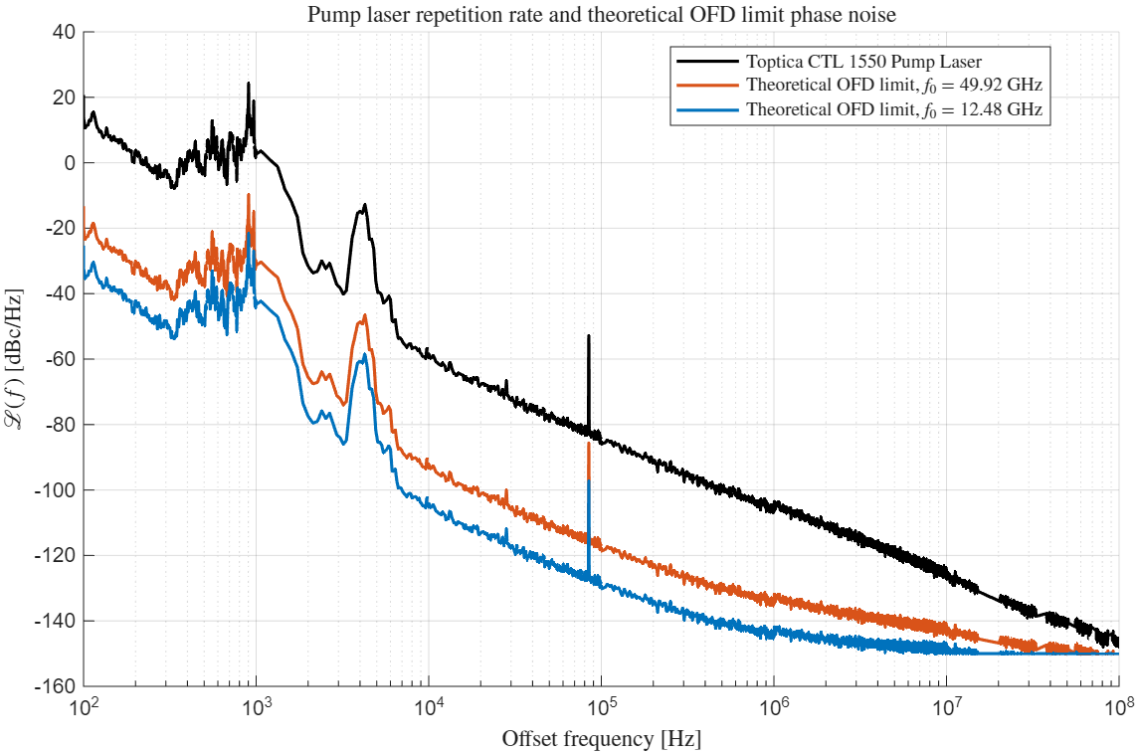

Figure 4.7: Pump laser repetition rate signal and theoretical OFD limit phase noise.

Figure 4.7 shows the phase noise of the pump laser repetition rate signal and calculated theoretical OFD limit, before and after scaling through ideal frequency division. Smoothing has been applied in the transition between estimated white phase noise floor.

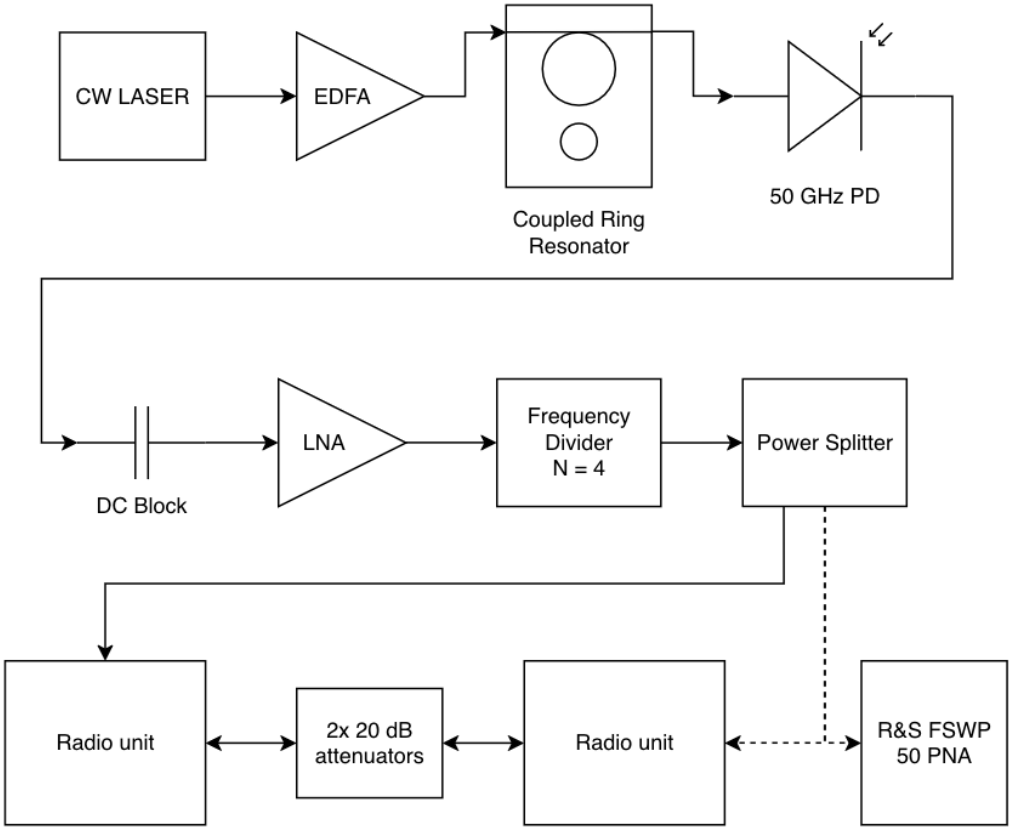

Figure 4.8: Optical oscillator implementation in radio test bed.

Figure 4.8 shows a simplified block diagram representation of the optical oscillator implemented in the radio test bed.

The Toptica CTL is used to generate CW signal at $\lambda_{opt} = 1560.9$ nm. After optical amplification using an Erbium-Doped Fiber Amplifier (EDFA), the signal is fed to the coupled ring resonator, generating the OFC (see section 3.1).

The resonator output is thereafter fed to the high speed photodetector, generating the RF signal through detection of the optical beat frequency at $f_0 \approx 49.92$ GHz.

Photodetectors typically introduce a DC bias to the output signal. A DC-blocking capacitor was therefore inserted after the photodetector in order to avoid damages to the LNA and subsequent RF stages.

After electrical amplification using the ADL8106 LNA, frequency division by 4 (N = 4) was performed using the AT-FDN-54AS2-FD. The FD output signal at $f_0 = 12.5$ GHz is input to a power splitter and the output signal branches of fed to the LO port on the modified RU's.

Three measurement series were conducted, hereafter referred to as Soliton State A, Soliton State B and Soliton State C or, for brevity, State A, State B, and State C, respectively.
Between measurement series, the number of Kerr solitons and pump laser power was modified. The number of Kerr solitons in State A was higher than that of State B and State C. The optical input power was not recorded during radio link measurements, but was seen to relate to the number of Kerr solitons. Communication link signal-to-interference-plus-noise-ratio (SINR) was observed using the RU software interface for bandwidths of 1000, 1500 and 2000 MHz. While maintaining the OFD conditions, the phase noise and power was measured by feeding one branch of the split LO signal to the Rohde & Schwarz PNA (indicated in Fig. 4.8 with a dotted line).

5

Results and Discussion

This chapter opens with the results of the phase noise characterization of the frequency divider. The results are subsequently discussed, and potential sources contributing to the observed noise are identified.

Next, the measured phase noise performance of the optical oscillator is compared with the corresponding theoretical estimation. By observing oscillator noise regions, a performance bottleneck is identified and discussed.

Finally, the optical oscillator is evaluated in a radio test bed and compared with conventional signal generators. The resulting communication link performance is analyzed, and the influence of the phase noise spectrum on system performance is discussed. Simulated noise-floor elevation is compared with measurement results and the impact of signal de-correlation is briefly examined.

5.1 Frequency divider

The frequency divider (FD) used was treated as a "black-box" of unknown phase noise performance and internal construction. Several performance metrics indicate that the FD is *static*, including

- wide input and output bandwidth,
- programmable division factor using logic level control voltage (CV) and
- differential operation.

Wideband injection-locked frequency dividers can be constructed, but impose significant bandwidth limitations as compared to static dividers [18].

Results presented in this section were obtained using the measurement configuration described in Fig. 4.1.

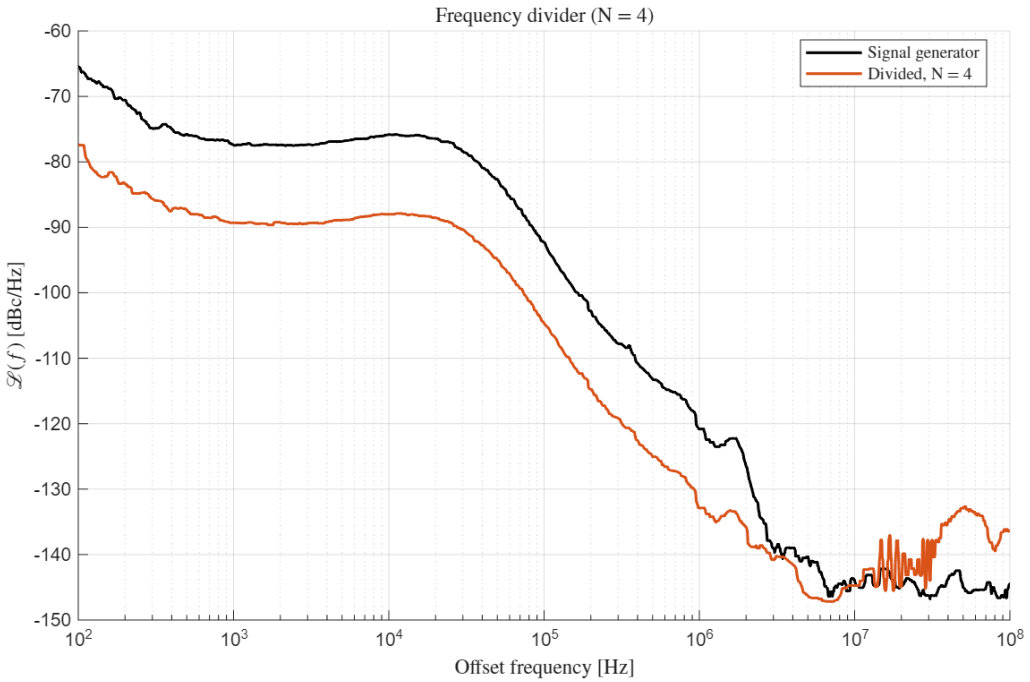

Figure 5.1: Phase noise before and after frequency division, division factor N = 4, f_{in} = 50 GHz, f_{out} = 12.5 GHz.

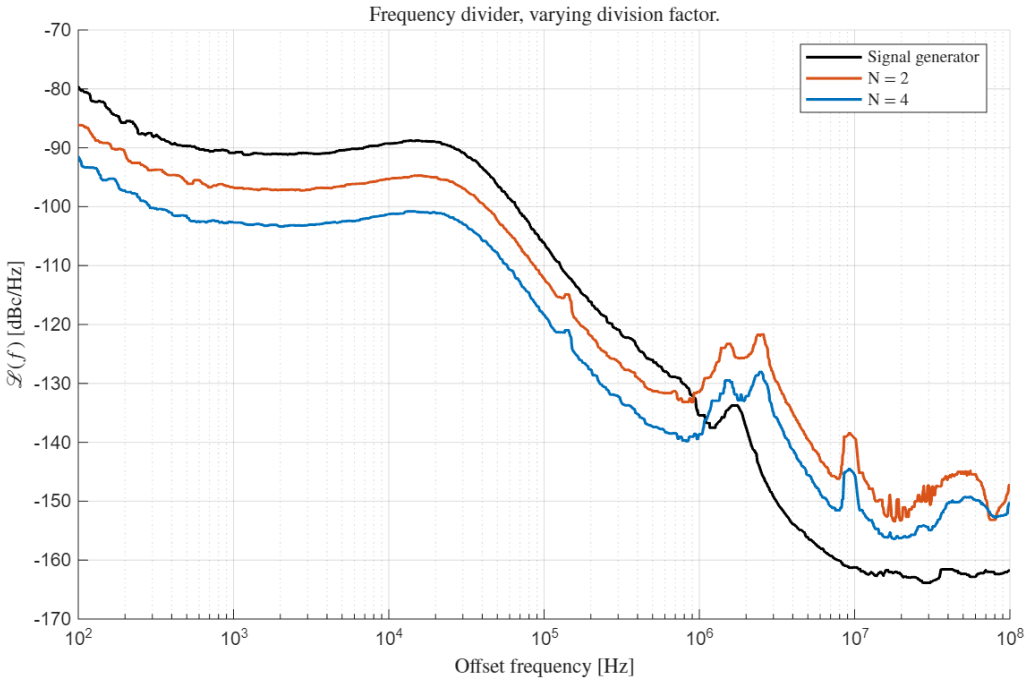

Figure 5.2: Phase noise before and after frequency division, division factors N = 2, 4, f_{in} = 10 GHz, f_{out} = 5 GHz and 2.5 GHz.

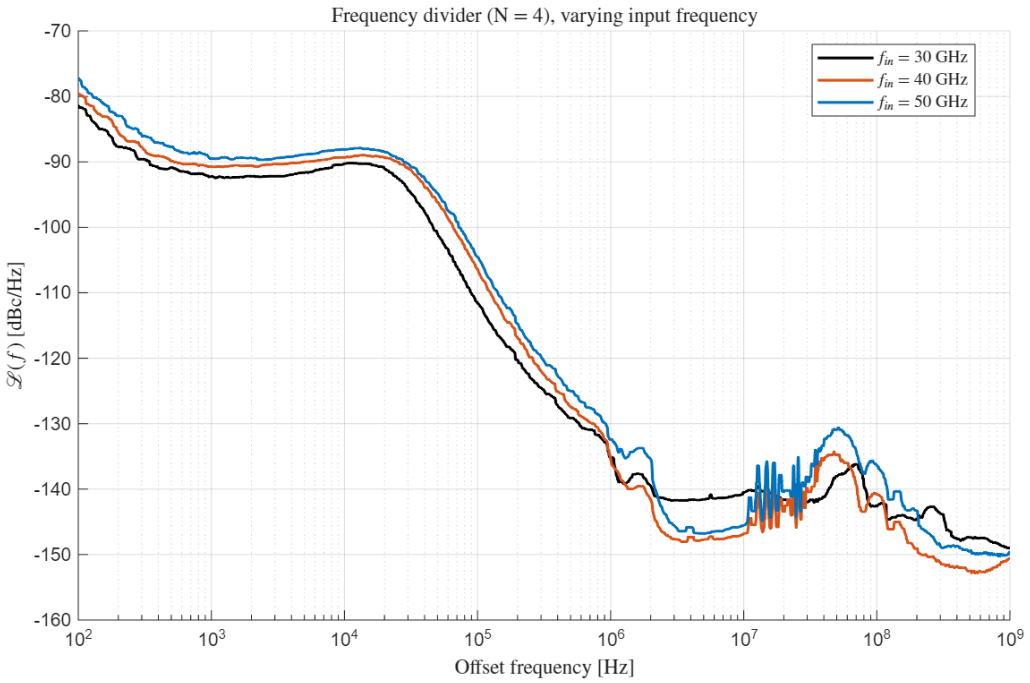

Figure 5.3: Phase noise after frequency division, division factor N = 4, f_{in} = 50 GHz, 40 GHz and 30 GHz.

Fig. 5.1 shows the input and output FD phase noise for an input signal frequency f_{in} = 50 GHz when division by 4 is performed. This corresponds closely to the frequency divider condition of operation when implemented in the optical oscillator radio test bed (Fig. 4.8).

In Fig. 5.2, the input and output FD phase noise is observed for division by 2 and 4. Fig. 5.3 shows FD output phase noise when f_{in} = 30 GHz, 40 GHz and 50 GHz.

The FD output phase noise roughly follows the theoretical estimated phase noise improvement of $-20\log_{10}(N)$ dB for $f \lesssim 1$ MHz for all measurement series. Described in section 2.3, the regions of slope $1/f^2$ (-20 db/decade) and higher originate in oscillator noise mechanisms and constitute correlated noise [31, 14].

In Fig. 5.1, a region of noise contribution is clearly visible at $f \approx 5$ MHz with a peak $\mathcal{L}(f) \approx -130$ dBc/Hz. The noise appears to consist of a significant amount of spurious noise, seen most clearly in Fig. 5.3 at $f \approx 20$ MHz. Previously explained in 2.1, spurs occurring at high frequency offsets may be incorrectly visualized due to the measurement equipment resolution bandwidth. It is likely that the observed noise consists of narrow-band periodic jitter.

An input voltage range of +5 V to +8 V can be used to power the device. Internal voltage regulation is therefore required, and the choice of regulator may have a significant effect on phase noise performance [34]. It is possible that spurious noise at $f \approx 20$ MHz is caused by a switching regulator. Spurious noise may also be caused by signal cross-talk in the clock signal feedback network.

A frequency dependence on the output noise profile can be seen in Fig. 5.3, where an input frequency of 30 GHz results in a noticeably different noise profile compared

to higher input signal frequencies. Variations in division factor does not appear to significantly impact the apparent noise contribution, as observed in Fig. 5.2.

As the divider operates on a wide input/output bandwidth, it is likely that frequency dependent output buffering amplification stages are employed. Amplification inherently introduces additive flicker- and white phase which could contribute to changes in output phase noise depending on input/output frequency. Assuming separate output buffering amplifiers, variations in physical proximity to a source of electromagnetic interference may introduce frequency-dependent spurious noise.

Due to the unknown topology of the FD used, definitive conclusions of noise mechanisms affecting observed phase noise cannot be drawn. Residual noise measurements were not performed, and the added phase noise of the FD can therefore not be quantified.

Limited data exists on wideband mmWave static frequency divider additive white phase noise for comparison. Static SCL divide-by-two in GaN HEMT technology has achieved far-out phase noise $<$ -155 dBc/Hz, (verified for) f_{in} = 1 GHz to 27 GHz [35].

5.2 Optical Oscillator

Results presented in this section were obtained using the measurement configuration described in Fig. 4.8.

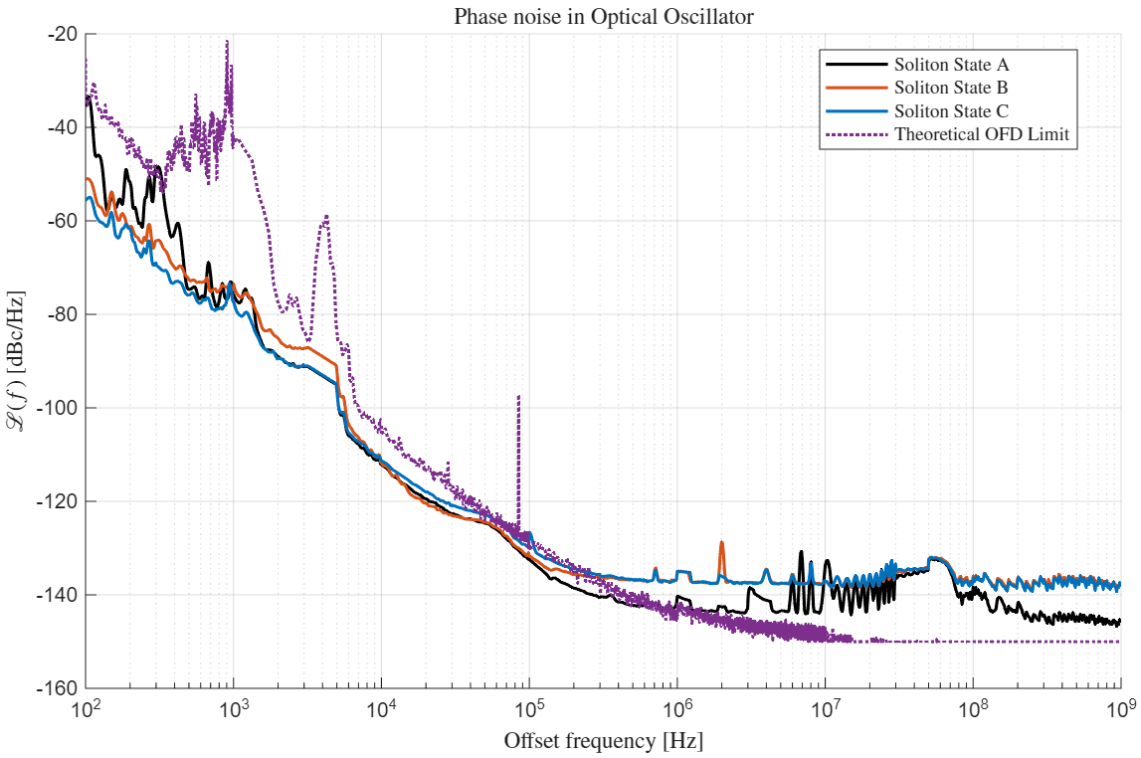

Figure 5.4: Optical oscillator and theoretical OFD limit phase noise, $f_0 = 12.48$ GHz.

In Fig. 5.4, the optical oscillator phase noise and theoretical OFD limit are compared. Although 2-point OFD was not implemented during radio test bed measurements, the theoretical OFD limit may still serve as a relevant benchmark. For offset frequencies $f < 1$ MHz, the implemented oscillator is seen to outperform the OFD estimation. The cause of this has not been fully determined. The *avoided mode crossing* produced by coupling between main and auxiliary rings of the photonic molecule may have mitigated the transfer of pump phase fluctuations to the optical frequency comb [39, 15].

Close-in phase noise is dominated by a $1/f^2$ dependence, with the $1/f$ region being negligible or not observable.

The phase noise floor of State A is approx. 5 dB higher than the estimated shot-noise limit of -150 dBc/Hz (see section 3.2.1). In comparison, State B and State C exhibit higher noise floors of approximately -140 dBc/Hz. State A maintained a higher number of Kerr solitons than State B and State C, resulting in higher optical power at the photodetector input. This indicates that increasing the optical power reduces the relative impact of shot noise, particularly in the far-out phase noise region.

Spurious noise introduced by the frequency divider is clearly visible for State A and partly obscured by the noise floor in State B and State C. White phase noise will have been introduced by the frequency divider and LNA. Applying (4.1) assuming typical operations with a microresonator conversion efficiency of -20 dB, $P_L = +10$ dBm and $F = 4$ dB, the additive white phase noise through amplification is

$$\mathcal{L}(f) = \frac{S_\phi(f)}{2} = \frac{F k_b T}{2P_0} \approx -163 \text{ dBc/Hz}. \tag{5.1}$$

Assuming a shot-noise floor of -150 dBc/Hz, the additive white phase noise of the amplifier will not contribute meaningfully.

5.3 Communication link

The measurements presented in this section were obtained using configurations described in 4.5 and 4.8 for signal generator (*Anritsu, Rohde & Schwarz*) and optical oscillator (*Soliton State A, Soliton State B and Soliton State C*) measurement series respectively.

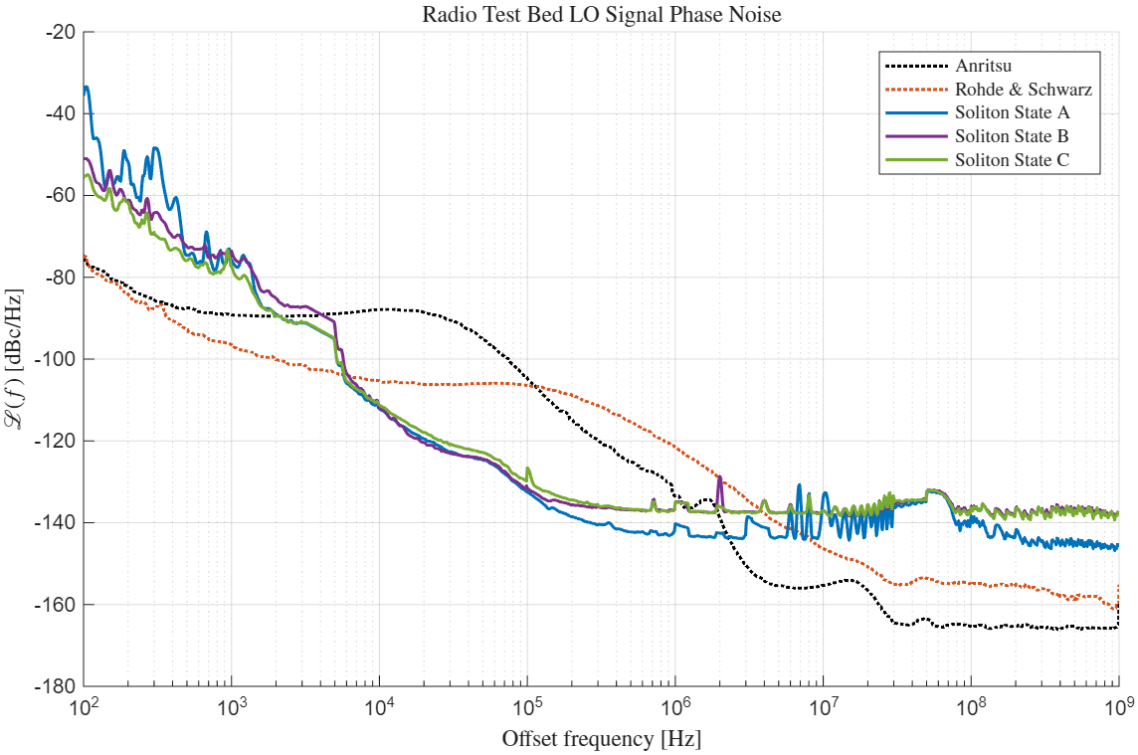

Figure 5.5: Radio test bed local oscillator phase noise, $f_0 = 12.5$ GHz.

A comparison of radio test bed LO phase noise is shown in Fig. 5.5. The Anritsu and Rohde & Schwarz signal generators generate the LO signal using a PLL, observable through the characteristically flat region within the PLL bandwidth. The optical oscillator, with its characteristic $1/f^2$ slope, manages to achieve superior performance for offset frequencies between approx. 8 kHz and 2 MHz. Notably, the optical oscillator white phase noise level is significantly higher than that of the signal generators used.

Tables 5.1, 5.2 and 5.3 show the link SINR, signal power at RU LO port, ϕ_{rms}, $J_{\phi,rms}$ and SNR_ϕ for link bandwidths and signal sources used. The RMS phase ϕ_{rms} was calculated using phase noise measurement data according to equation (2.4). The upper noise integration limit was chosen to match the link bandwidth B as $f_b = B/2$, assuming equality between the upper- and lower-sideband phase noise. The lower integration limit f_a in equation (2.4) is limited by phase noise measurement data starting at an offset frequency of 100 Hz. The RMS jitter and SNR_ϕ are calculated using equations (2.6) and (2.5) respectively. Communication link SINR values were recorded using the RU software interface.

Table 5.1: Radio test bed link performance, $B = 1000$ MHz.

Setup	SINR [dB]	P_{LO} [dBm]	SNR_ϕ [dB] $f_a = 100$ Hz	SNR_ϕ [dB] $f_a = 1$ kHz	SNR_ϕ [dB] $f_a = 100$ kHz
Internal	34.2	-	-	-	-
Anritsu	34.7	-0.2	39.19	39.39	55.18
Anritsu, LNA	31.9	-12.8	37.63	37.76	42.70
Rohde & Schwarz	32.5	-4.9	47.30	48.13	50.04
Soliton State A	26.2	-11.9	19.42	44.81	50.85
Soliton State B	23.6	-13.0	31.19	42.37	46.59
Soliton State C	22.6	-14.5	34.52	44.59	46.87

Table 5.2: Radio test bed link performance, $B = 1500$ MHz.

Setup	SINR [dB]	P_{LO} [dBm]	SNR_ϕ [dB] $f_a = 100$ Hz	SNR_ϕ [dB] $f_a = 1$ kHz	SNR_ϕ [dB] $f_a = 100$ kHz
Internal	32.0	-	-	-	-
Anritsu	32.9	-0.2	39.19	39.39	55.16
Anritsu, LNA	30.8	-12.8	37.63	37.75	42.68
Rohde & Schwarz	32.3	-4.9	47.28	48.11	50.00
Soliton State A	26.0	-11.9	19.42	44.61	50.09
Soliton State B	23.5	-13.0	31.13	41.65	44.90
Soliton State C	22.2	-14.5	34.40	43.53	45.20

Table 5.3: Radio test bed link performance, $B = 2000$ MHz.

Setup	SINR [dB]	P_{LO} [dBm]	SNR_ϕ [dB] $f_a = 100$ Hz	SNR_ϕ [dB] $f_a = 1$ kHz	SNR_ϕ [dB] $f_a = 100$ kHz
Internal	31.2	-	-	-	-
Anritsu	32.1	-0.2	39.19	39.39	55.14
Anritsu, LNA	30.5	-12.8	37.62	37.74	42.66
Rohde & Schwarz	31.8	-4.9	47.27	48.09	49.98
Soliton State A	26.0	-11.9	19.42	44.45	49.54
Soliton State B	23.1	-13.0	31.09	41.15	43.90
Soliton State C	21.7	-14.5	34.31	42.82	44.19

Using the results above, two observations are made:

The SNR_ϕ and link SINR are most closely correlated at $f_a = 100$ kHz.

The dependency on integration limit in correlating phase noise and link SINR is most clearly seen when comparing State A, State B and State C. For all system bandwidths, State C achieved the highest link SINR. Still, for $f_a = 100$ Hz, State A SNR_ϕ is lower than that of State B and State C, indicating a higher level of phase noise for low offset frequencies. This can be observed in Fig. 5.5, where State A exhibits the highest phase noise for offset frequencies below 1 kHz.

Further indication of integration limit dependency is seen when observing the measurement series Anritsu. Anritsu achieved the highest SINR, notably surpassing the internal LO. Still, for $f_a = 100$ Hz and $f_a = 1$ kHz, the Anritsu SNR_ϕ is lower than that of other measurement series. Notably, $\mathrm{SNR}_{\phi,\mathrm{Anritsu}} < \mathrm{SNR}_{\phi,\mathrm{State\ C}}$ for $f_a = 1$ kHz.

These results indicate that low offset phase noise is rejected. Such rejection is likely achieved through receiver *clock recovery*.

Clock and data recovery (CDR) is widely used in asynchronous communication systems to mitigate the impact of phase noise and timing jitter on link performance. Various architectures exist for implementing CDR, among which PLLs are one of the most commonly used [30]. For PLLs, the jitter transfer function is a critical metric is which relates to the PLL loop bandwidth [21]. One possible explanation for the correlation between link SINR and SNR_ϕ being heavily influenced by choice of lower integration limit may therefore be a corresponding PLL clock recovery circuit, rejecting phase noise for frequency offsets within its bandwidth. CDR may also be performed digitally using a digital phase-locked loop (DPLL).

Link SINR **cannot be correlated to** SNR_ϕ **solely by choice of integration limits.**

The lowest link SINR occurred for State C. However, State C exhibits a higher SNR_ϕ for all system bandwidths and integration limits as compared to State B. Link performance is therefore not exclusively determined by the phase noise of the injected LO signal. Notably, the LO carrier power for State C is lower than that of State B. Both are significantly lower than the nominal output power of the internal LO.

The influence of AM noise on a timing signal depends on the input waveform slope [9]. To maximize the slope at the sampling instant, the LO clock signal is commonly driven into compression in the mixing stage, generating a square-wave-like signal. Since the internal operation of the LO signal path in the radio unit is not known, insufficient input power may prevent the signal from reaching the required compression level. It therefore cannot be excluded that amplitude noise was introduced, which may influence link SINR. However, it is unlikely to have resulted in significant signal degradation.

Analysis of optical oscillator performance

When used as an LO source during radio test bed measurements, the optical oscillator achieved a lower link SINR relative to the signal generators and internal RU PLL. It should be noted that the signal generators, as well as the internal RU PLL, achieve low phase noise compared to most commercially available synthesizers.

The main limitation in optical oscillator implementation is likely to originate in photodetection. This is supported by the observed increased white noise floor when a lower optical signal power was delivered to the photodetector input, relating to the reduction of optical power generated for lesser number of solitons states in measurement series State B and State C compared to State A. However, this estimations is based on a very simplified model of shot-noise in photodetection. Accurate shot noise modeling could improve estimation confidence [27].

In ultrashort, picosecond pulse detection, relative intensity noise (RIN) may significantly influence phase noise performance. For device dependent photocurrents however, the AM-to-PM coefficient α, (described in equation (3.7)), can be nulled [36]. Careful attention should be given in future system implementation to ensure minimal noise contribution.

The additive white phase noise due to the inclusion of the frequency divider (FD) could not be quantified or reliably estimated. Given knowledge of device implementation, the noise contributions may be estimated [9]. Spurious noise was introduced by the FD, the source of which is unknown. As electromagnetic interference from power supply noise and signal cross-talk is known to occur in digital circuits [33], these sources of noise are deemed likely.

Amplification using the LNA introduced additive white phase noise. The relative level was found to be low compared to the observed optical oscillator noise floor and as such, it likely had minor influence on link performance.

5.3.1 Noise Floor Elevation and De-correlation

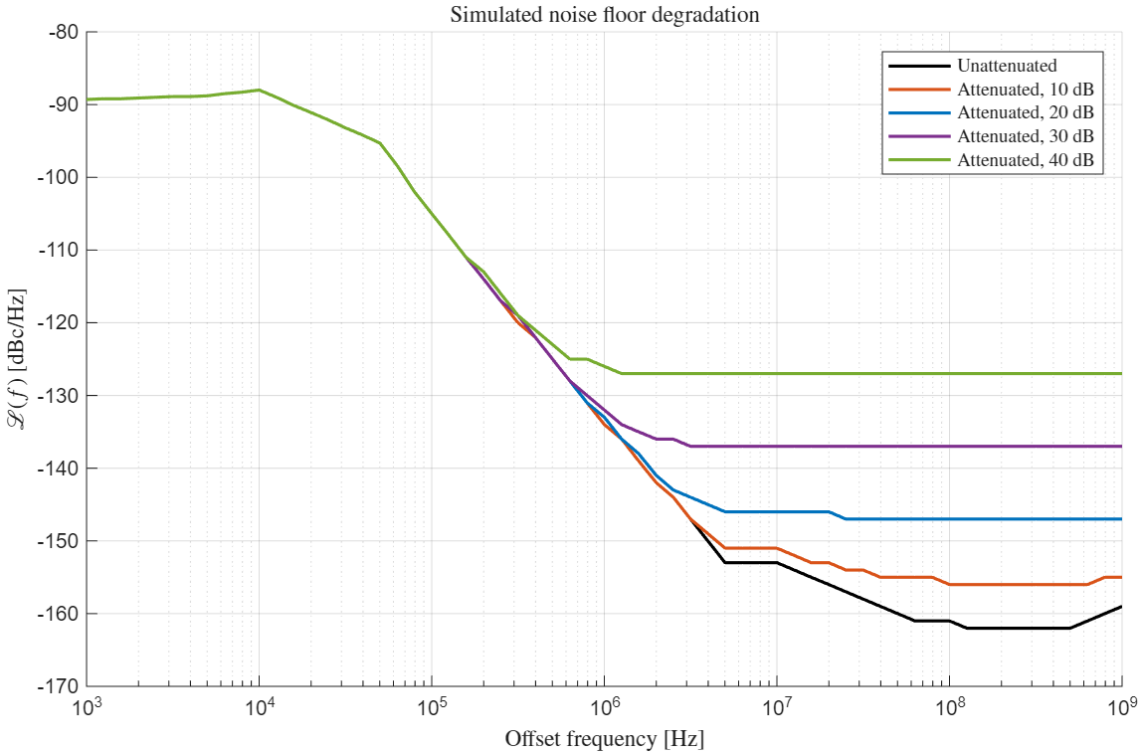

Figure 5.6: Simulated noise floor elevation with varied attenuation and amplification.

Figure 5.6 shows the result of simulated noise floor elevation as detailed in section 2.3.1 for attenuation and amplification of 10 dB, 20 dB, 30 dB and 40 dB. The carrier power was set to -10 dBm (estimating measured LO signal power), with a system simulation temperature of 290 K.

Using equation (4.1), the noise floor is $\mathcal{L}(f) = k_B T/2P_0 \approx -167$ dBc/Hz.

In Table 5.4, the relationship between the level of attenuation applied and SNR_ϕ is presented for bandwidths of 100, 1000, 1500 and 2000 MHz is shown, $f_a = 100$ kHz.

Table 5.4: Noise floor elevation simulation, $f_a = 100$ kHz.

Attenuation [dB]	SNR_ϕ [dB] $B = 100$ MHz	SNR_ϕ [dB] $B = 1000$ MHz	SNR_ϕ [dB] $B = 1500$ MHz	SNR_ϕ [dB] $B = 2000$ MHz
0	54.66	54.60	54.56	54.46
10	54.64	54.41	54.27	54.02
20	54.42	52.97	52.24	51.28
30	53.02	47.15	45.44	43.63
40	47.15	37.90	35.93	33.95

Measurements of noise floor elevation were obtained using the configuration referred to as *Correlated, SHF 806 E* in section 4.3.

Table 5.5 presents the measured link SINR for different combinations of signal generator model, output carrier power, and communication bandwidth.

Table 5.5: Noise floor elevation in radio test bed.

Configuration	SINR, Unmodified [dB]	SINR, Attenuated [dB]
$B = 1000$ MHz		
Anritsu MG3695B		
$P = -5$ dBm	31.5	30.7
$P = 0$ dBm	33.4	33.1
$P = 10$ dBm	34.7	34.7
Rohde & Schwarz SMB100A		
$P = -5$ dBm	27.9	28.8
$P = 0$ dBm	31.1	30.9
$P = 10$ dBm	32.5	32.3
$B = 1500$ MHz		
Anritsu MG3695B		
$P = -5$ dBm	31.0	29.4
$P = 0$ dBm	32.2	33.7
$P = 10$ dBm	32.9	32.8
Rohde & Schwarz SMB100A		
$P = -5$ dBm	29.7	28.7
$P = 0$ dBm	31.2	30.9
$P = 10$ dBm	32.3	32.3
$B = 2000$ MHz		
Anritsu MG3695B		
$P = -5$ dBm	30.3	28.7
$P = 0$ dBm	31.1	30.8
$P = 10$ dBm	32.0	32.0
Rohde & Schwarz SMB100A		
$P = -5$ dBm	29.6	28.4
$P = 0$ dBm	30.9	30.4
$P = 10$ dBm	31.8	31.8

Observing simulation results in Table 5.4 for an attenuation of 20 dB, a minor performance is seen. Measurement results in Table 5.5 indicate minimal impact on radio link SINR. LO signal phase noise measurements were not performed. It is therefore difficult to draw conclusions regarding the efficacy of the method applied. Similar approaches have been successfully employed in previous studies, incorporating multiple stages of attenuation and amplification. [5].

Signal de-correlation was performed as described in section 4.3 by altering the transmission line length of one branch in the split LO signal.

In Table 5.6, the link SINR for the de-correlated LO signal is compared to the correlated LO signal link SINR. No clear trend can be observed, with a maximum SINR deviation of −0.6 dB to +1.1 dB before/after de-correlation was performed.

Table 5.6: LO signal de-correlation in radio test bed.

Configuration	SINR, Correlated [dB]	SINR, De-correlated [dB]
$B = 1000$ MHz		
Anritsu MG3695B		
$P = -5$ dBm	31.5	32.3
$P = 0$ dBm	33.4	34.0
$P = 10$ dBm	34.7	34.8
Rohde & Schwarz SMB100A		
$P = -5$ dBm	27.9	28.8
$P = 0$ dBm	31.1	31.6
$P = 10$ dBm	32.5	33.6
$B = 1500$ MHz		
Anritsu MG3695B		
$P = -5$ dBm	31.0	31.2
$P = 0$ dBm	32.2	32.3
$P = 10$ dBm	32.9	32.9
Rohde & Schwarz SMB100A		
$P = -5$ dBm	29.7	29.4
$P = 0$ dBm	31.2	30.9
$P = 10$ dBm	32.3	31.7
$B = 2000$ MHz		
Anritsu MG3695B		
$P = -5$ dBm	30.3	30.5
$P = 0$ dBm	31.1	31.6
$P = 10$ dBm	32.0	32.1
Rohde & Schwarz SMB100A		
$P = -5$ dBm	29.6	29.4
$P = 0$ dBm	30.9	30.8
$P = 10$ dBm	31.8	31.5

6

Conclusion

This work presents the integration and evaluation of a Kerr-microresonator optical frequency division local oscillator (LO) for wireless communication applications.

Results suggest that photodetection constituted the primary performance limitation of the optical oscillator implementation. Significant shot noise levels were observed, limited by the power-handling capability of the photodetector. Amplitude-to-phase noise conversion of pump-laser relative intensity noise may also have contributed to the elevated phase noise floor, although this effect was not examined in this work.

A frequency divider and amplifier was used to integrate the optical oscillator into a radio test bed. The noise contributions from these devices could not be quantified, due to a lack of residual noise measurements. Calculations of white noise introduced during amplification indicate minor system influence. While not conclusively verified, results indicate that noise introduced by photodetection dominated oscillator performance rather than the frequency divider and amplifier.

Integrated LO phase noise was found to correlate closely with observed radio link performance, given appropriate choice of integration limits. The importance of integration limits is believed to relate to clock recovery circuits. Given radio unit application knowledge, communication can be estimated from phase noise measurements. It was, however, not possible to fully exclude the inclusion of amplitude noise introduced during measurements; possibly reducing the reliability of link performance estimation using integrated phase noise.

Recommended Future Work

Further investigation is needed to assess OFD in wireless communication systems. Research on high-speed photodetectors with increased power handling capabilities is ongoing [25]. Investigating possible mitigation of photodiode shot-noise using high power handling high-speed photodetectors may therefore lead to further insight on noise mechanisms in OFD implementations.

Bibliography

[1] R. Adler. "A Study of Locking Phenomena in Oscillators". In: *Proceedings of the IRE* 34.6 (1946), pp. 351–357. DOI: 10.1109/JRPROC.1946.229930.

[2] Inc Analog Devices. *ADL8106 Datasheet*. Feb. 2023. URL: https://www.analog.com/media/en/technical-documentation/data-sheets/adl8106.pdf.

[3] Daniel Benedikovič et al. "Recent advances in integrated photonics: introduction". In: *J. Opt. Soc. Am. B* 42.11 (Nov. 2025), RAI1–RAI3. DOI: 10.1364/JOSAB.582187. URL: https://opg.optica.org/josab/abstract.cfm?URI=josab-42-11-RAI1.

[4] Romain Bouchand et al. "Accurate control of optoelectronic amplitude to phase noise conversion in photodetection of ultra-fast optical pulses". In: *Opt. Express* 25.11 (May 2017), pp. 12268–12281. DOI: 10.1364/OE.25.012268. URL: https://opg.optica.org/oe/abstract.cfm?URI=oe-25-11-12268.

[5] Jingjing Chen et al. "Influence of White LO Noise on Wideband Communication". In: *IEEE Transactions on Microwave Theory and Techniques* 66.7 (2018), pp. 3349–3359. DOI: 10.1109/TMTT.2018.2814040.

[6] Coherent. [Accessed 04-06-2026]. 2023. URL: https://www.coherent.com/resources/datasheet/networking/50ghz-photodetector-ds.pdf.

[7] J.D. Crockett and M. Siccardi. "Power supply noise conversion to phase noise in CMOS frequency digital divider". In: *Proceedings of the 2002 IEEE International Frequency Control Symposium and PDA Exhibition (Cat. No.02CH37234)*. 2002, pp. 699–702. DOI: 10.1109/FREQ.2002.1075971.

[8] J. Davila-Rodriguez et al. "Optimizing the linearity in high-speed photodiodes". In: *Opt. Express* 26.23 (Nov. 2018), pp. 30532–30545. DOI: 10.1364/OE.26.030532. URL: https://opg.optica.org/oe/abstract.cfm?URI=oe-26-23-30532.

[9] W.F. Egan. "Modeling phase noise in frequency dividers". In: *IEEE Transactions on Ultrasonics, Ferroelectrics, and Frequency Control* 37.4 (1990), pp. 307–315. DOI: 10.1109/58.56498.

[10] William F. Egan. *Phase-Lock Basics*. John Wiley I& Sons, Ltd, 2007. ISBN: 9780470118009. DOI: https://doi.org/10.1002/9780470178737.

[11] T M Fortier et al. "Generation of ultrastable microwaves via optical frequency division". In: *Nature Photonics* 5.7 (July 2011), pp. 425–429. DOI: https://doi.org/10.1038/nphoton.2011.121.

[12] Lou Frenzel. *What's the difference between the third-order intercept and the 1-DB compression points?* Oct. 2013. URL: https://www.electronicdesign.

com/resources/whats-the-difference-between/article/21799714/whats-the-difference-between-the-third-order-intercept-and-the-1-db-compression-points.

[13] A. Hajimiri. "Noise in phase-locked loops". In: *2001 Southwest Symposium on Mixed-Signal Design (Cat. No.01EX475)*. 2001, pp. 1–6. DOI: 10.1109/SSMSD.2001.914927.

[14] A. Hajimiri and T.H. Lee. "A general theory of phase noise in electrical oscillators". In: *IEEE Journal of Solid-State Circuits* 33.2 (1998), pp. 179–194. DOI: 10.1109/4.658619.

[15] Ó. B. Helgason I. Rebolledo-Salgado and V. Torres-Company. "Photonic molecule microcombs at 50 GHz repetition rate". In: *Conference on Lasers and Electro-Optics*. San Jose, California United States: Optica Publishing Group, 2022, p. 1. DOI: https://doi.org/10.1364/CLEO_SI.2022.SW4O.8.

[16] "IEEE Standard Definitions of Physical Quantities for Fundamental Frequency and Time Metrology–Random Instabilities". In: *IEEE Std 1139-2022 (Revision of IEEE Std 1139-2008)* (2022), pp. 1–60. DOI: 10.1109/IEEESTD.2022.9973001.

[17] "IEEE Standard for Jitter and Phase Noise". In: *IEEE Std 2414-2020* (2021), pp. 1–42. DOI: 10.1109/IEEESTD.2021.9364950.

[18] Alireza Imani and Hossein Hashemi. "Distributed Injection-Locked Frequency Dividers". In: *IEEE Journal of Solid-State Circuits* 52.8 (2017), pp. 2083–2093. DOI: 10.1109/JSSC.2017.2701325.

[19] Qing-Xin Ji et al. "Dispersive-wave-agile optical frequency division". In: *Nature Photonics* 19.6 (June 2025), pp. 624–629. ISSN: 1749-4893. DOI: 10.1038/s41566-025-01667-4. URL: https://doi.org/10.1038/s41566-025-01667-4.

[20] T. J. Kippenberg, R. Holzwarth, and S. A. Diddams. "Microresonator-Based Optical Frequency Combs". In: *Science* 332.6029 (2011), pp. 555–559. DOI: 10.1126/science.1193968. URL: https://www.science.org/doi/abs/10.1126/science.1193968.

[21] G Le Cheminant. *PLL Characterization for Data Communication Components and Systems*. Feb. 2024. URL: https://www.signalintegrityjournal.com/articles/3475-pll-characterization-for-datacommunication-components-and-systems.

[22] D.B. Leeson. "A simple model of feedback oscillator noise spectrum". In: *Proceedings of the IEEE* 54.2 (1966), pp. 329–330. DOI: 10.1109/PROC.1966.4682.

[23] S. Levantino et al. "Phase noise in digital frequency dividers". In: *IEEE Journal of Solid-State Circuits* 39.5 (2004), pp. 775–784. DOI: 10.1109/JSSC.2004.826338.

[24] Shanghai AT Microwave Limited. *AT-FD-54AS2-FD Datasheet*. Jan. 2024. URL: https://www.atmicrowave.com/uploads/PDF/AT-FDN-54AS2-FD.pdf.

[25] David Marpaung, Jianping Yao, and José Capmany. "Integrated microwave photonics". In: *Nature Photonics* 13.2 (Feb. 2019), pp. 80–90. ISSN: 1749-4893. DOI: 10.1038/s41566-018-0310-5. URL: https://doi.org/10.1038/s41566-018-0310-5.

[26] David M. Pozar. *Microwave engineering*. 4th ed. OCLC: ocn714728044. Hoboken, NJ: Wiley, 2012. ISBN: 978-0-470-63155-3.

[27] Franklyn Quinlan et al. "Analysis of shot noise in the detection of ultrashort optical pulse trains". In: *J. Opt. Soc. Am. B* 30.6 (June 2013), pp. 1775–1785. DOI: 10.1364/JOSAB.30.001775. URL: https://opg.optica.org/josab/abstract.cfm?URI=josab-30-6-1775.

[28] H.R. Rategh and T.H. Lee. "Superharmonic injection-locked frequency dividers". In: *IEEE Journal of Solid-State Circuits* 34.6 (1999), pp. 813–821. DOI: 10.1109/4.766815.

[29] B. Razavi. "A study of phase noise in CMOS oscillators". In: *IEEE Journal of Solid-State Circuits* 31.3 (1996), pp. 331–343. DOI: 10.1109/4.494195.

[30] B. Razavi. "Challenges in the design high-speed clock and data recovery circuits". In: *IEEE Communications Magazine* 40.8 (2002), pp. 94–101. DOI: 10.1109/MCOM.2002.1024421.

[31] E Rubiola. *Phase Noise and Frequency Stability*. [Accessed 23-05-2026]. 2025. URL: https://rubiola.org/pdf-lectures/Scient-Instrum-Files/Phase%20noise%20Wiley%2C%20Ch2%20updated%20draft.pdf.

[32] Kashif Siddiq et al. "Phase Noise in FMCW Radar Systems". In: *IEEE Transactions on Aerospace and Electronic Systems* 55.1 (2019), pp. 70–81. DOI: 10.1109/TAES.2018.2847999.

[33] Inc. Skyworks Solutions. *A primer on jittter, jitter measurement and phase-locked loops*. [Accessed 29-05-2026]. 2021. URL: https://www.skyworksinc.com/-/media/Skyworks/SL/documents/public/application-notes/AN687.pdf?utm_source=copilot.com.

[34] M Sternberg et al. *How to Select the Best Power Solution for RF Signal Chain Phase Noise Performance*. [Accessed 30-05-2026]. 2021. URL: https://www.analog.com/en/resources/technical-articles/how-to-select-the-best-power-solution.html.

[35] F. Strömbeck et al. "A Static Frequency Divider in GaN HEMT Technology". In: *2021 51st European Microwave Conference (EuMC)*. 2022, pp. 309–312. DOI: 10.23919/EuMC50147.2022.9784244.

[36] J. Taylor et al. "Characterization of Power-to-Phase Conversion in High-Speed P-I-N Photodiodes". In: *IEEE Photonics Journal* 3.1 (2011), pp. 140–151. DOI: 10.1109/JPHOT.2011.2109703.

[37] Georg Böck Ulrich L. Rohde Ajay Kumar Poddar. *The Design of Modern Microwave Oscillators for Wireless Applications*. John Wiley I& Sons, Ltd, 2005. ISBN: 9780471727170. DOI: https://doi.org/10.1002/0471727172.ch2. URL: https://onlinelibrary.wiley.com/doi/abs/10.1002/0471727172.ch2.

[38] Wanghua Wu, Robert Bogdan Staszewski, and John R. Long. "Chapter 3 - Circuit Design Techniques for mm-Wave Frequency Synthesizer". In: *Millimeter-Wave Digitally Intensive Frequency Generation in CMOS*. Academic Press, 2016, pp. 35–55. ISBN: 978-0-12-802207-8. DOI: https://doi.org/10.1016/B978-0-12-802207-8.00003-4. URL: https://www.sciencedirect.com/science/article/pii/B9780128022078000034.

[39] Xiaoxiao Xue et al. “Mode-locked dark pulse Kerr combs in normal-dispersion microresonators”. In: *Nature Photonics* 9.9 (Sept. 2015), pp. 594–600. ISSN: 1749-4893. DOI: 10.1038/nphoton.2015.137. URL: https://doi.org/10.1038/nphoton.2015.137.

[40] Jianping Yao. “Microwave Photonics”. In: *Journal of Lightwave Technology* 27.3 (2009), pp. 314–335. DOI: 10.1109/JLT.2008.2009551.

[41] Hao Zhang et al. “Coherent optical frequency combs: From principles to applications”. In: *Journal of Electronic Science and Technology* 20.2 (2022), p. 100157. ISSN: 1674-862X. DOI: https://doi.org/10.1016/j.jnlest.2022.100157. URL: https://www.sciencedirect.com/science/article/pii/S1674862X22000106.

DEPARTMENT OF ELECTRICAL ENGINEERING
CHALMERS UNIVERSITY OF TECHNOLOGY
Gothenburg, Sweden 2026
www.chalmers.se

CHALMERS
UNIVERSITY OF TECHNOLOGY